Title - Rescue of aberrant huntingtin palmitoylation ameliorates mutant huntingtin-induced toxicity

Authors – Fanny L. Lemarié[a], Nicholas S. Caron[a], Shaun S. Sanders[a,b], Mandi E. Schmidt[a], Yen T.N. Nguyen[a], Yun Ko[a], Xiaohong Xu[d,e], Mahmoud A. Pouladi[a,d], Dale D.O. Martin[a,c], Michael R. Hayden[a]*

[a] Centre for Molecular Medicine and Therapeutics, BC Children's Hospital Research Institute, University of British Columbia, Vancouver, Canada

[b] Department of Molecular and Cellular Biology, University of Guelph, Guelph, Canada

[c] Department of Biology, University of Waterloo, Waterloo, Canada

[d] Translational Laboratory in Genetic Medicine, Department of Physiology, Yong Loo Lin School of Medicine, National University of Singapore, Singapore

[e] Department of Neurology and Stroke Center, The First Affiliated Hospital, Jinan University, Guangzhou, China

*To whom correspondence should be addressed (mrh@cmmt.ubc.ca)
Centre for Molecular Medicine and Therapeutics
BC Children's Hospital Research Institute
University of British Columbia
3025-950 West 28th Ave
Vancouver, BC Canada
V5Z 4H4
604-875-3535
mrh@cmmt.ubc.ca

Highlights:

- Palmitoylation of mHTT is reduced in multiple transgenic HD mouse models
- HTT palmitoylation decreases with increasing polyQ length in HD patient cells
- mHTT-lowering in mouse brains does not rescue aberrant palmitoylation
- mHTT palmitoylation in HD patient-derived cells can be rescued via APT inhibition
- Promoting palmitoylation reduces mHTT aggregation and cytotoxicity *in vitro*

30 **Abstract:** Huntington disease (HD) is a neurodegenerative disorder caused by a CAG
31 expansion in the *HTT* gene that codes for an elongated polyglutamine tract in the
32 huntingtin (HTT) protein. HTT is subject to multiple posttranslational modifications (PTMs)
33 that regulate its cellular function. Mutating specific PTM sites within mutant HTT (mHTT)
34 in HD mouse models can modulate disease phenotypes, highlighting the key role of HTT
35 PTMs in the pathogenesis of HD. These findings have led to increased interest in
36 developing small molecules to modulate HTT PTMs in order to decrease mHTT toxicity.
37 However, the therapeutic efficacy of pharmacological modulation of HTT PTMs in
38 preclinical HD models remains unknown. HTT is palmitoylated at cysteine 214 by the
39 huntingtin-interacting protein 14 (HIP14 or ZDHHC17) and 14-like (HIP14L or ZDHHC13)
40 acyltransferases. Here, we assessed if HTT palmitoylation should be regarded as a
41 therapeutic target to treat HD by (1) investigating palmitoylation dysregulation in
42 humanized rodent and human HD model systems, (2) measuring the impact of mHTT-
43 lowering therapy on brain palmitoylation, and (3) evaluating if HTT palmitoylation can be
44 modulated by pharmacological intervention. We show that palmitoylation of mHTT and
45 some HIP14/HIP14L-substrates is decreased early in multiple HD mouse models, and
46 that aging further reduces HTT palmitoylation. Lowering mHTT in the brain of YAC128
47 mice is not sufficient to rescue aberrant palmitoylation. However, we demonstrate that
48 mHTT palmitoylation can be normalized in COS-7 cells, in YAC128 cortico-striatal primary
49 neurons and HD patient-derived lymphoblasts using an acyl-protein thioesterase (APT)
50 inhibitor. Moreover, we show that modulating palmitoylation reduces mHTT aggregation
51 and mHTT-induced cytotoxicity in COS-7 cells and YAC128 neurons.

52 **Keywords:** Palmitoylation, S-acylation, huntingtin, Huntington disease, ZDHHC17, acyl-
53 protein thioesterase, neuroprotection

54 **Abbreviations:** ABE, acyl-biotin exchange assay; APT, acyl-protein thioesterase; ASO,
55 antisense oligonucleotide; HD, Huntington disease; hiPSC, human induced pluripotent
56 stem cell; HIP14, huntingtin-interacting protein 14 (ZDHHC17); HIP14L, huntingtin-
57 interacting protein 14-like (ZDHHC13); HTT, huntingtin (human); Htt, huntingtin (mouse);
58 ICV, intracerebroventricular; LNA, locked nucleic acid; mHTT, mutant huntingtin; NEM,
59 N-ethylmaleimide; PalmB, palmostatin B; PAT, palmitoyl acyltransferase; PTM, post-
60 translational modification

61 **1. Introduction**

62 Huntington disease (HD) is an inherited neurodegenerative disorder characterized
63 by involuntary movements, behavioural changes and cognitive impairment. There are
64 currently no therapies available to influence its inexorable progression (Caron et al., 2018;
65 Evans et al., 2013; Fisher and Hayden, 2014; Myers, 2004). The genetic cause of HD is
66 an expanded CAG-repeat tract (>35 repeats) in the *HTT* gene leading to an abnormally
67 long polyglutamine (polyQ) tract in the huntingtin (HTT) protein.

68 HTT interacts with numerous protein partners and is involved in many cellular processes,
69 including endocytosis, vesicle/organelle transport and recycling, autophagy, and DNA
70 transcription (Maiuri et al., 2017; Ochaba et al., 2014; Saudou and Humbert, 2016). HTT
71 is subjected to numerous post-translational modifications (PTMs), including
72 phosphorylation (Aiken et al., 2009; Humbert et al., 2002; Schilling et al., 2006),
73 acetylation (Jeong et al., 2009), ubiquitination (Kalchman et al., 1996), SUMOylation
74 (Steffan et al., 2004), proteolysis (Graham et al., 2006), and fatty acylation (palmitoylation
75 and myristoylation) (D. D. O. Martin et al., 2018; Martin et al., 2014; Yanai et al., 2006).
76 These PTMs regulate subcellular localization, protein-protein interactions, aggregation
77 and clearance which modulates the toxicity of mutant HTT (mHTT) (Atwal et al., 2007;
78 Cariulo et al., 2017; Caron et al., 2013; Kratter et al., 2016; Lontay et al., 2020).

79 In the presence of the HD mutation, levels of several key PTMs are significantly altered
80 *in vitro* and *in vivo* (Cariulo et al., 2020, 2017; Warby et al., 2005). Introducing mutations
81 at specific PTM sites of mHTT has been shown to modulate disease phenotypes in
82 various HD models. Blocking proteolysis of mHTT at aspartic acid 586 (D586) prevents
83 striatal neurodegeneration in the YAC128 HD mouse model (Graham et al., 2006).

84 Reducing phosphorylation at serine residues 13/16 or 421 (S13/16A, S421A) in the
85 BACHD mouse model and HD human induced pluripotent stem cell (hiPSC)-derived
86 neural cells exacerbates disease phenotypes. In contrast, mimicking phosphorylation at
87 these residues (S13/16D, S421D) prevents neurodegeneration (Gu et al., 2009; Kratter
88 et al., 2016; Xu et al., 2020). These findings highlight the key role of HTT PTMs in the
89 pathogenesis of HD and have stimulated interest in the development of drugs to modulate
90 HTT PTMs in order to decrease mHTT levels and toxicity. To date, most research has
91 focused on normalizing HTT phosphorylation at S13 and S16, and preventing mHTT
92 proteolysis (Aharony et al., 2015; Atwal et al., 2011; Bowie et al., 2018).

93 Palmitoylation refers to the addition of a palmitic acid (C16:0) onto a cysteine
94 residue via a thioester bond. This process is catalyzed by a family of palmitoyl
95 acyltransferases (PATs). Palmitoylation increases the hydrophobicity of proteins, and
96 therefore plays a key role in protein trafficking, stability, membrane association and
97 protein-protein interactions (Fukata and Fukata, 2010). It is the most common protein-
98 lipid modification in the brain (Smotrys and Linder, 2004). Most importantly, it is reversible
99 and allows for dynamic regulation of protein functions at the synapse, thus playing an
100 important role in neurodevelopmental processes and in neuronal survival (Globa and
101 Bamji, 2017; Hubalkova et al., 2021; Matt et al., 2019; Mukai et al., 2008). Disruption of
102 protein palmitoylation has been implicated in the pathogenesis of several neurological
103 disorders, including Alzheimer's disease, schizophrenia and intellectual disability (Cho
104 and Park, 2016; Sanders et al., 2015b).

105 We first described that HTT is palmitoylated at cysteine 214 (C214), a reaction catalyzed
106 by the palmitoyl acyltransferases ZDHHC17 and ZDHHC13, also known as huntingtin-

107 interacting protein 14 and 14-like (HIP14 and HIP14L) (Yanai et al., 2006). In the presence
108 of the HD mutation, mHTT was found to be less palmitoylated in the brain of the YAC128
109 HD mouse model (Yanai et al., 2006). Transient expression of mHTT carrying a
110 palmitoylation-resistant mutation (C214 to serine, C214S) in immortalized cell lines and
111 primary neurons led to increased aggregates and nuclear inclusion formation, increased
112 cell death and increased susceptibility to excitotoxicity (Yanai et al., 2006).
113 Autopalmitoylation of HIP14 and HIP14L, and palmitoylation of many of their synaptic
114 substrates were also downregulated in the YAC128 HD mouse brains or in the brains of
115 mice lacking one *Htt* allele (*Htt*$^{+/-}$) (Huang et al., 2011; Singaraja et al., 2011). Moreover,
116 mouse models deficient in either HIP14 (*Hip14*$^{-/-}$) or HIP14L (*Hip14l*$^{-/-}$) develop
117 neuropathological deficits that are reminiscent of HD (Sutton et al., 2013), and loss of
118 both *Hip14* and *Hip14l* leads to embryonic lethality (Sanders et al., 2016, 2015a).
119 Collectively, these findings link defects in fatty acylation with neuronal dysfunction and
120 neurodegeneration in HD. However, the effect of palmitoylation on HTT function and the
121 role that loss of HTT palmitoylation plays in the pathogenesis of HD are still not fully
122 elucidated.

123 In this study, we investigate whether palmitoylation is dysregulated in HD mouse
124 models and human HD samples. We also evaluate whether pharmacological modulation
125 of mHTT palmitoylation represents a potential therapeutic target for the treatment of HD.

126 **2. Materials and methods**

127 **2.1. Materials**

128 **2.1.1. Reagents and chemicals**

129 **Table 1** lists the reagents and chemicals used for this study along with the application,
130 manufacturer and catalogue number.

131 **2.1.2. Antibodies**

132 **Table 2** displays the list of antibodies used along with the application, concentrations and
133 experimental conditions.

134 **2.1.3. Experimental models**

135 **HD mouse lines** - Heterozygous YAC128 (line 53), homozygous YAC128 (line 55),
136 homozygous YAC18 (line 60), BACHD, humanized Hu18/18 and Hu97/18, humanized
137 Hu21/21 and Hu128/21 mice were maintained on the FVB/N background. The description
138 of the HD mouse lines used is displayed in **Table 3**. The YAC128 model expresses two
139 mouse Htt alleles and the full length human mHTT transgene (Slow et al., 2003). The
140 BACHD model expresses two mouse Htt alleles and the full length human mHTT
141 transgene (Gray et al., 2008). The two humanized Hu97/18 and Hu128/21 models
142 express only full length human WT and mHTT transgenes (Southwell et al., 2017, 2013).
143 Experiments were performed according to protocols approved by the University of British
144 Columbia Animal Care Committee (experimental protocol 2016/2020 #A20-0107,
145 breeding protocol #A20-0233). Homozygous YAC128 and YAC18 mice were used for the
146 neuronal culture, to improve culture health by avoiding an overnight genotyping step. For

147 all cohorts, approximately equal numbers of male and female mice were used. All mice
148 were sacrificed using CO_2 asphyxiation in accordance with UBC SOP #I012.

149 **Cell line culture** – Control and HD patient-derived lymphoblastoid cell lines (**Table 4**)
150 were obtained from the NIGMS Human Genetic Cell Repository at the Coriell Institute for
151 Medical Research. All cell lines were maintained in RPMI 1640 medium containing 10%
152 FBS, 2 mM GlutaMAX, 10 units/mL of penicillin and 10 µg/mL of streptomycin. Cells were
153 grown in T-25 flasks incubated in an upright position with vented caps at 37°C and 5%
154 CO_2. Cell density was kept between 2.10^5 and 5.10^5 cells/mL of media.

155 COS-7 cells were grown in DMEM medium supplemented with 10% FBS, 1 mM sodium
156 pyruvate, 2 mM GlutaMAX, 10 units/mL of penicillin and 10 µg/mL of streptomycin. Cells
157 were grown in 10-cm plates at 37°C and 5% CO_2, and were split using a 0.25% trypsin
158 solution (1:10 dilution) when cells were ~90% confluent by microscopy.

159 Human pluripotent stem cells (hPSCs) lines listed in **Table 5** were cultured on Matrigel-
160 coated plates in mTeSR-1 complete medium supplemented with 10 units/mL of penicillin
161 and 10 µg/mL of streptomycin at 37°C and 5% CO_2, and were split with ReLeSR.

162 **Neuronal culture** - Timed pregnancies were set up by mating homozygous YAC18 (line
163 60) or YAC128 (line 55) mice. At E16.5, embryos were removed from pregnant females.
164 Cortical and striatal tissues attached were dissected in ice-cold HBSS, gently dissociated
165 with a P1000 pipette (×2-3 times) and briefly spun. Tissues were digested in 0.05%
166 trypsin-EDTA for 8 min at 37°C until addition of 10% FBS in neurobasal (NB) medium, as
167 previously described (Schmidt et al., 2020). Cells were centrifuged, further dissociated by
168 mechanical trituration in NB medium (supplemented with B27, GlutaMAX, penicillin and
169 streptomycin) and DNase (0.08 mg/mL). Neurons were plated in 6-well Nunclon Delta

170 surface plates at a density of 1.10^6 cells/well in 2 mL of complete NB medium. Prior to
171 plating, 6-well plates were coated with sterile-filtered 50 µg/mL of poly-D-lysine
172 hydrobromide for 2 h at room temperature and washed four times with sterile water. All
173 cultures were regularly supplemented with fresh complete NB medium (20% well volume).

174 **2.2. Methods**

175 **2.2.1. Plasmid transfection**

176 COS-7 cells were seeded in 6-well or 96-well plates overnight at 37°C and 5% CO_2. The
177 next day, cells were transfected with cDNA plasmid constructs encoding for 15Q and
178 mutant 128Q N-terminus HTT_{1-548} (N548), HTT_{1-1212} (N1212) and full-length HTT_{1-3144}
179 (HTT), or 17Q and 138Q HTT_{1-588}-YFP (N588) using X-tremeGENE 9 DNA transfection
180 reagent (ratio 3:1, reagent (µL): DNA (µg)). Cells were treated or harvested 18 to 24h
181 post-transfection.

182 **2.2.2. Acyl-protein thioesterase (APT) inhibition with palmostatin B**

183 ***Inhibition of APTs in immortalized cell lines***

184 At 18-24h post-transfection, COS-7 cells were deprived of lipid for 1 h in DMEM (without
185 methionine or cysteine) supplemented with 5% Charcoal stripped FBS, subsequently
186 treated with DMSO or 15 µM Palmostatin B (PalmB) (diluted in DMSO at 1000X on
187 InSolution) while concurrently metabolically labelled with 100 µM alkyne-palmitate for 6h.
188 Bio-orthogonal click chemistry of alkyne-palmitate was performed as subsequently
189 described in section §2.2.4.

190 ***Inhibition of APTs in primary neurons***

191 Primary neurons from cortex and striatum of E16.5 mouse embryos (homozygous YAC18
192 and YAC128 mouse lines) were cultured as previously described in section §2.1.3. At

193 DIV10, neuronal cultures were treated with DMSO or with 15 μM PalmB (InSolution) for
194 6h. The ABE assay was performed on neuronal lysates as described in section §2.2.4.

195 ***Inhibition of APTs in control and HD patient-derived lymphoblastoid lines***

196 Lymphoblasts were cultured as previously described in section §2.1.3. Cells were seeded
197 at a density of 600,000 cells/2 mL/well in 6 well plates. The next day, cells were treated
198 with DMSO or 10 μM PalmB for 4h. The ABE assay was performed on lymphoblasts as
199 described in section §2.2.4.

200 **2.2.3. Intracerebroventricular HTT antisense oligonucleotide infusion**

201 A fully phosphorothioate modified gapmer ASO with 5' locked nucleic acid (LNA)
202 modifications in each wing, matching a sequence in intron 22 of the *HTT* gene (5'-
203 TAATACGTAAGTGTCACAA-3', custom synthesized by Qiagen) was delivered by
204 intracerebroventricular (ICV) injection as previously described (Southwell et al., 2015).
205 Five-month-old YAC128 (line 53) mice were anesthetized using 3% isoflurane and
206 secured on a stereotaxic frame. Mice were given pre-operative subcutaneous
207 buprenorphine (0.1 mg/kg) and 0.25% bupivacaine at the site of incision. A midline
208 incision was made in the scalp to expose the skull. Then, a 50 μL Hamilton syringe with
209 a 26-gauge needle was oriented to the bregma and moved 0.3 mm anterior, 1 mm lateral,
210 and 3 mm ventral. An injection volume of 10 μL was delivered into the lateral ventricle at
211 a rate of 5 μL/min. Mice were either injected with 50 μg ASO in sterile PBS (n=7) or PBS
212 only (n=6). The needle was left in place for 2 min after injection, before being slowly
213 retracted. The scalp was closed with sutures and Vetbond tissue adhesive. Animals were
214 then placed in a recovery cage with a heating pad, hydrogel, and food on the cage floor.
215 Mice were given post-operative buprenorphine as needed and monitored for 72h. Brains

216 were collected a month later, when mHTT levels have been shown to be lowered by 70
217 to 90% (Southwell et al., 2015).

218 **2.2.4. Palmitoylation assays**

219 ***Acyl-biotin exchange (ABE) assay***

220 **Mouse brain** - ABE assays were performed on whole or half frozen brain samples from
221 YAC128 (line 53) and WT littermate controls, BACHD and WT littermate controls,
222 Hu97/18 and Hu18/18, Hu128/21 and Hu21/21, as previously described (Drisdel and
223 Green, 2004; Huang et al., 2009). Briefly, brains were harvested and immediately snap-
224 frozen in liquid N_2 and stored at -80°C until being processed. Frozen brains were
225 homogenized on ice in lysis buffer (150 mM NaCl, 50 mM Tris, 5 mM EDTA, 0.1% SDS,
226 1% triton X-100, pH 7.4) with 100 mM NEM (4 mL lysis buffer/brain hemisphere).
227 Homogenates were sonicated for 15 sec at 30% power to shear DNA and the insoluble
228 material was removed by centrifugation at 20,000 × g for 15 min at +4°C. Protein
229 concentrations in lysates were assessed by DC protein assay. HTT, PSD95, and GAD65
230 were immunoprecipitated (IP) from brain lysates (300 µL) by overnight incubation with
231 Protein G Dynabeads or PureProteome protein A/G, and appropriate antibodies for
232 immunoprecipitation (**Table 2**). Beads were then washed and split into two and treated
233 either with neutral pH hydroxylamine (HAM+) in lysis buffer or just lysis buffer (HAM-) for
234 2h for HTT and 1h for the other three proteins at room temperature. Following HAM
235 treatment, beads were washed and treated with 2.5 µM EZ-Link BMCC-Biotin in pH 6.2
236 lysis buffer for 1h at 4°C. At the end of the BMCC-Biotin treatment, beads were washed
237 and heated at 70°C for 10 min with NuPAGE LDS sample buffer and 100 mM DTT to
238 elute proteins.

239 **Control and HD-patient derived lymphoblastoid and hiPSC lines** – Lymphoblastoid
240 aggregates in suspension in the media were dissociated by trituration and centrifuged for
241 5 min at 500 × g at room temperature. HiPSCs were washed with DMEM/F12, lifted from
242 plated using ReLeSR and spun at 500 × g for 5 min at +4°C. Supernatant was discarded
243 and cell pellets were frozen until being processed, as previously described for mouse
244 brain samples. HTT was immunoprecipitated from cell lysates by overnight incubation
245 with Protein G Dynabeads and HTT (MAB2166) antibodies (approx. 250 µg protein and
246 2 µL MAB2166 for 20 µL beads).

247 ***Bio-orthogonal labelling assay using alkyne-palmitate***

248 **Immortalized cell lines** - cells transiently transfected with cDNA HTT constructs were
249 deprived of lipid during 1 h incubation in DMEM supplemented with 5% charcoal stripped
250 FBS 18h post-transfection and subsequently metabolically labelled with 100 µM alkyne-
251 palmitate for 6 h. Cells were lifted from plates in PBS using cell scrapers, pelleted by
252 centrifugation (500 × g, 5 min, +4°C) and subsequently lysed in RIPA (150 mM $NaCl_2$, 5
253 mM M EDTA, 50 mM Tris, 1% NP-40, 0.5% sodium deoxycholate, 0.1% SDS in dH_2O,
254 complete protease inhibitors cocktails) or SDP lysis (50 mM Tris pH 8.0, 150 mM NaCl,
255 1% Igepal, 40 mM NaF, 1 mM PMSF, 2 mM sodium vanadate, complete protease
256 inhibitors cocktails) buffer for 10 min on ice, 5 min at 4°C on rotator and were centrifuged
257 (16,000 × g, 10 min, 4°C). Bio-orthogonal click chemistry of alkyne-palmitate was
258 performed, as previously described (Yap et al., 2010) on cell lysates immunoprecipitated
259 with anti-HTT antibodies (BKP1 or MAB2166). HTT immunoprecipitates were adjusted to
260 1% SDS and incubated with 100 mM TBTA, 1 mM $CuSO_4$, 1 mM TCEP and 100 mM
261 azido-biotin at +37°C in darkness for 1 h.

262 **2.2.5. Western blot analysis**

263 Brain, COS-7 and HD patient-derived hiPSC and lymphoblastoid supernatants from HTT
264 assays were run on NuPAGE™ 3-8% Tris-Acetate gradient protein gels in Tris-Acetate
265 SDS Running Buffer (50 mM Tricine, 50 mM Tris Base, 0.1% SDS, pH 8.24) or
266 homemade 8% low bis acrylamide (1:200 bis-acrylamide:acrylamide) gels in SDS-Tris-
267 glycine running buffer (25 mM Tris base, 190 mM glycine, 3.5 mM SDS) (Carroll et al.,
268 2011) to resolve full length HTT alleles with small ΔQs. Brain lysates from the other
269 proteins (SNAP25, PSD95 and GAD65) were run on homemade tris-glycine gels (7-12%)
270 in SDS-Tris-glycine running buffer. Protein were transferred to 0.45 µm nitrocellulose.
271 Membranes were blocked with 5% milk in Phosphate-Buffered Saline (PBS) or 3-5% BSA
272 in Tris-Buffered Saline (TBS) supplemented with 0.1-0.5% Tween-20 (T). Primary
273 antibody dilutions of HTT (D7F7 or MAB2166), SNAP25 polyclonal, PSD95 monoclonal,
274 and GAD65 polyclonal in 3-5% BSA PBST or TBST were applied to the immunoblots at
275 room temperature for 1h or overnight at +4°C (**Table 2**). Membranes were washed 4 × 5
276 min in PBST or TBST. The appropriate secondary antibodies and Alexa Fluor 680
277 conjugated streptavidin were applied in 3-5% BSA PBST or TBST for 1 to 2h at room
278 temperature. Membranes were washed 4 × 5 min in PBST or TBST and imaged using
279 the LI-COR Odyssey Infrared Imaging System (Li-Cor Biosciences). Densitometry was
280 quantified using the LiCor Image Studio Lite software and median signal intensity
281 following background subtraction was used for analysis. Palmitoylation was analyzed as
282 a ratio of HAM+ palmitoylation signal to total immunoprecipitated protein signal and
283 normalized to the control.

284 **2.2.6. Aggregation and cytotoxicity assays**

285 ***Filter retardation assay***

286 Protein aggregation of insoluble HTT_{1-588}-YFP transiently expressed in COS-7 cells was
287 measured using the filter-trap retardation assay, as previously described (Dale D. O.
288 Martin et al., 2018; Wanker et al., 1999). After 72 h of transfection, COS-7 cells expressing
289 the indicated HTT_{1-588}-YFP constructs and treated with 15 µM PalmB for 48h were lysed
290 in lysis buffer (50 mM Tris pH 8.8, 100 mM NaCl, 5 mM $MgCl_2$, 0.5% Igepal CA630, 1 mM
291 EDTA with 1X cOmplete protease inhibitor cocktail and 25 unit/mL benzonase fresh)
292 (~150 µL/cell pellet) for 30 min on ice without vortexing or spinning (only pipetting to
293 homogenize). Protein concentrations in lysates were assessed by DC protein assay and
294 adjusted to 1 µg/µL in a total volume of 50 µL. Samples (50 µg of proteins) were denatured
295 in a 1:1 volume of denaturation buffer (2% SDS and 50 mM DTT) at 98°C for 10 min.
296 Denatured samples were loaded in duplicate over a 0.2 µm cellulose acetate (OE66)
297 membrane positioned in the filter retardation apparatus (Whatman, The Convertible
298 filtration manifold system cat. Series 1055). The membrane was washed with a 0.2% SDS
299 solution once prior to loading the samples, and twice after (100 µL/wash). The membrane
300 was blocked in 3% BSA TBST (0.1% Tween 20) for an hour and probed by standard
301 immunoblotting analysis with primary mouse anti-HTT (MAB2166) and rabbit anti-GFP
302 antibodies, followed by secondary antibodies and detection using the LI-COR Odyssey
303 immunoblotting system. The quantity of aggregates retained on the filter expressed was
304 measured with Image Studio Lite and calculated relatively to the PBS control group
305 (arbitrarily set at 1) and technical replicates were averaged.

306 ***LDH activity cytotoxicity assay***

307 Cytotoxicity was assessed in COS-7 transiently expressing human HTT or YAC128
308 neurons after 6 and 24h of PalmB treatment, using the CYQUANT LDH cytotoxicity assay
309 kit, as per the manufacturer's guidelines. Lactate dehydrogenase (LDH) is a well-defined
310 and reliable indicator of cytotoxicity. Extracellular LDH was here quantified by a coupled
311 enzymatic reaction in which LDH catalyzes the conversion of lactate to pyruvate via NAD+
312 reduction to NADH. This can be measured by using an excitation of 560 nm and an
313 emission of 590 nm. A cell density of 10,000 cells/well was chosen after experimental
314 optimization. Fluorescence was read on an EnSpire 2300 Multilabel plate reader from
315 PerkinElmer using the EnSpire manager software. Cytotoxicity (in %) was calculated
316 using the formula:

317 $$\%\,Cytotoxicity = \left(\frac{Compound\ treated\ LDH\ activity^{1} - Spontaneous\ LDH\ activity^{2}}{Maximum\ LDH\ activity^{3} - Spontaneous\ LDH\ activity^{2}}\right) \times 100$$

318 [1] fluorescence in transfected COS-7 cells or YAC128 neurons treated with PalmB (x%),
319 [2] fluorescence in untransfected COS-7 cells untreated or YAC128 neurons treated with DMSO (0%),
320 [3] fluorescence in untransfected COS-7 cells or YAC128 neurons treated with 10X lysis buffer (100%).

321 **2.2.7. Statistical Analysis**

322 GraphPad Prism 9 was used for all statistical analysis and graph preparation. Figures
323 were generated in Adobe illustrator 2020. All data are presented as mean ± SEM.
324 Biological replicates (n) are displayed on each graph, or indicated in the captions.
325 Student's t-test or 1- or 2-way ANOVA statistical tests with post-hoc analysis (Tukey,
326 Dunnett, Sidak or Bonferroni) were used for all experiments. In some cases, t-tests were
327 performed between specific groups after an ANOVA test when a planned comparison
328 was established during the experimental design process. Significance for these tests is
329 noted with the "#" symbol instead of "*".

330 **3. Results**

331 **3.1. Palmitoylation levels of HTT and HIP14/HIP14L substrates are decreased in the**
332 **BACHD and in two humanized HD mouse models**

333 We first wanted to assess in a low throughput, high confidence manner how the
334 presence of mHTT impacts protein palmitoylation in multiple mouse models of HD,
335 including BACHD, YAC128, Hu97/18 and Hu128/21 (**Table 3**). We therefore compared
336 levels of palmitoylation of HTT, HIP14 and/or HIP14L substrates 25 kDa synaptosomal-
337 associated protein (SNAP25), 95 kDa post-synaptic density protein (PSD95), and 65 kDa
338 glutamate decarboxylase (GAD65) in the brains of 6-month-old HD mouse lines and their
339 respective control line (**Figure 1**).

340 In the BACHD model (**Figure 1.B**), the palmitoylation level of mHTT Q97 was
341 significantly lower (70%) than palmitoylation of mouse Htt Q7 in the WT or HD brains (1-
342 way ANOVA (1WA): $p<0.0001$; Tukey's post-test (Tk): $p<0.0001$ for Q97 vs. Q7 in WT or
343 HD brains). In the humanized Hu97/18 and Hu18/18 brains (**Figure 1.C** - 1WA:
344 $p=0.0002$), the palmitoylation level of mHTT Q97 was significantly lower than wtHTT Q18
345 in the Hu97/18 (50%; Tk: $p=0.0002$) and Hu18/18 (40%; Tk: $p=0.0023$) brains. In the
346 Hu128/21 and Hu21/21 brains (**Figure 1.D** - 1WA: $p<0.0001$), the palmitoylation level of
347 mHTT Q128 was significantly lower than wtHTT Q21 in the Hu128/21 (20%; Tk:
348 $p=0.0004$) and Hu21/21 (30%; Tk: <0.0001) brains. In the YAC128 model (**Figure 1.A** -
349 1WA: $p<0.0001$), palmitoylation of mHTT Q128 was significantly decreased compared to
350 endogenous mouse Htt Q7 expressed in the YAC128 brain (60%; Tk: $p<0.0001$) and in
351 the WT littermate control brain (70%; Tk: $p<0.0001$), consistent with the 80% decrease of
352 mHTT Q128 compared to wtHTT Q18 in the YAC18 brain (Yanai et al., 2006).

353 HIP14 (ZDHHC17) and HIP14L (ZDHHC13) show substrate specificity for
354 neuronal proteins, including SNAP25, PSD95, and GAD65 (Huang et al., 2004), which all
355 play important roles in synaptic transmission. We therefore assessed palmitoylation levels
356 of these proteins in all four HD mouse models. SNAP25 palmitoylation was decreased by
357 30% in the YAC128 brain (**Figure 1.E** - Student's test, p=0.031), 40% in the BACHD brain
358 (**Figure 1.F** - p=0.0017), 45% in the Hu97/18 brain (**Figure 1.G** - p=0.041) and 20% in
359 the Hu128/21 brain (**Figure 1.H** - p=0.029) compared to their respective controls. PSD95
360 palmitoylation was also significantly decreased in the YAC128 brain (**Figure 1.I** - 35%;
361 p<0.0001) and the BACHD brain (**Figure 1.J** - 25%; p=0.020) compared to WT littermate
362 control brains. PSD95 palmitoylation showed a trend towards being reduced in the
363 Hu97/18 brain (**Figure 1.K** - 23%; p=0.10), but was unchanged in the Hu128/21 brain
364 (**Figure 1.L** - p=0.98) compared to controls. In contrast, palmitoylation of GAD65 was
365 unchanged in the YAC128, BACHD and Hu97/18 mouse models (**Figure 1.M-N-O**), but
366 was decreased by 15% in the brain of Hu128/21 (**Figure 1.P** - p=0.043) compared to the
367 Hu21/21 mice.

368 Our data shows that palmitoylation levels of HTT and various HIP14/14L
369 substrates are reproducibly reduced in all four HD mouse models. The absence of
370 endogenous Htt in the humanized HD brain does not exacerbate protein palmitoylation
371 dysregulation but may reveal subtle differences in palmitoylation dysregulation for GAD65
372 and PSD95.

373 **3.2. Palmitoylation of mutant HTT is decreased early in the brain of the humanized**
374 **HD mouse model, Hu128/21**

375 Our next goal was to investigate if aging affects palmitoylation of HTT in the brain
376 of humanized Hu128/21 HD mice. Palmitoylation of wtHTT and mHTT in the brain of
377 Hu21/21 and Hu128/21 mice at 1, 3, 6 and 12 months of age was measured using the
378 ABE assay (**Figure 2.A-B-C-D**). At all the ages investigated, the palmitoylation level of
379 mHTT was significantly lower compared to wtHTT in either the Hu21/21 brain (30-40%)
380 or the Hu128/21 brain (20-40%) (1WA: $p<0.01$ at 1 and 3 months, $p<0.001$ at 6 and 12
381 months). Notably, the decreased palmitoylation of mHTT was most pronounced at 6 and
382 12 months of age (**Figure 2.C and D**).

383 We then directly compared palmitoylation levels of wt and mHTT at different ages
384 in Hu21/21 (**Figure 2.E**) or Hu128/21 brain lysates (**Figure 2.F**) and found that
385 palmitoylation levels of wtHTT (1WA, $p=0.0022$) and mHTT (2-way ANOVA (2WA),
386 $p<0.0001$) significantly declined with age, reaching a 30% decrease at 12 months
387 compared to wt and mHTT palmitoylation levels at 1 month. This decline of HTT
388 palmitoylation with age was observed for both wt and mHTT protein, independent of the
389 presence of the HD mutation in the mouse brain. Taken together, our data demonstrates
390 that palmitoylation of HTT is decreased with age and further decreased in the presence
391 of the HD mutation as early as 1 month of age in the humanized Hu128/21 HD mouse
392 model.

393 **3.3. HTT palmitoylation levels in human lymphoblasts decrease with increasing**
394 **polyQ tract length**

395 To further characterize palmitoylation dysregulation in HD, we assessed the impact
396 of the polyQ tract length on HTT palmitoylation in control and HD patient lymphoblasts
397 (**Figure 3.A, Table 4**). In the control lymphoblasts, wtHTT polyQ tracts were
398 approximately 17Qs in length. In the HD lymphoblasts, we stratified samples into two sub-
399 groups where mHTT polyQ tract lengths were either approximately 44Q or above 59Q.
400 The wtHTT protein in the HD lines had polyQ tracts with 17Qs.

401 We quantified the palmitoylation levels of wt or mHTT separately (**Figure 3.B**) or
402 HTT (wt and mHTT together) global palmitoylation level (**Figure 3.C**) and observed that
403 mHTT and global HTT palmitoylation levels were significantly decreased with increased
404 polyQ tract length (1WA: (**B**) p=0.027, Tk: p=0.016 for mHTT (>59Q) vs. wtHTT (17Q)
405 and p=0.057 for mHTT (>59Q) vs. wtHTT (~44Q); (**C**) p=0.037, Tk: p=0.031 for total
406 HTT(>59Q) vs. total HTT (17Q)). The exponential relationship between the global
407 palmitoylation level of HTT (wt and mHTT together) and the polyQ tract length (high
408 polyQ) in each lymphoblastoid line is displayed in **Figure 3.D** and supports a negative
409 linear relationship between the two parameters (correlation, p(two-tailed) =0.018).

410 Palmitoylation levels were also investigated in isogenic HD human pluripotent stem cells
411 (hPSCs) previously generated (Ooi et al., 2019; Xu et al., 2017) using the ABE assay
412 (**Figure 3.E**). The exponential relationship between the global palmitoylation level of HTT
413 (WT and mHTT together) and the polyQ tract length (high polyQ) in each hPSC line
414 (**Figure 3.F**) suggests a negative linear relationship between palmitoylation and polyQ
415 length without reaching statistical significance (correlation, p(two-tailed) =0.14).

416 Our findings in patient-derived cell lines further validate the impact of the HD
417 mutation on HTT palmitoylation level and suggest that palmitoylation levels of wt and
418 mHTT decreases with increasing polyQ length.

419 **3.4 ASO-mediated mHTT lowering in the brain of the YAC128 HD mouse model does**
420 **not rescue palmitoylation of HIP14 and HIP14L synaptic substrates**

421 We next wanted to evaluate the impact of mHTT lowering in the CNS on
422 palmitoylation and function of synaptic proteins. Five-month-old YAC128 mice received
423 intracerebroventricular (ICV) injection of either PBS (n=6) or an ASO targeting human
424 HTT (HTT-ASO; n=7) (Southwell et al., 2015). Brains were collected 1 month later, and
425 palmitoylation of HTT, SNAP25, PSD95 and GAD65 was measured using the ABE assay
426 (**Figure 4**). As expected, mHTT levels were lowered by approximately 90%, whereas
427 levels of mouse Htt remained unchanged (**Figure 4.A**).

428 We measured a 30% reduction of mHTT palmitoylation compared to mouse Htt
429 (2WA: $p<0.0001$, HD mutation, $p<0.0001$) in the PBS controls (Tk: $p=0.049$) and a 60%
430 reduction in the ASO treated animals (Tk: $p<0.0001$), but the ASO treatment did not
431 change Htt and mHTT palmitoylation levels (**Figure 4.B**). ASO treatment also did not
432 significantly alter the palmitoylation level of SNAP25 (**Figure 4.C**), PSD95 (**Figure 4.D**)
433 and GAD65 (**Figure 4.E**). Taken together, mHTT lowering in the brain of the YAC128
434 mouse did not rescue aberrant palmitoylation of the proteins examined.

435 **3.5. Inhibition of APT increases palmitoylation levels of HTT in COS-7 cells, YAC128**
436 **cortico-striatal primary neurons and HD patient-derived lymphoblasts**

437 Since ASO-mediated mHTT lowering *in vivo* did not rescue the reduced
438 palmitoylation observed in YAC128 brains, we hypothesized that promoting this
439 modification pharmacologically may represent a relevant therapeutic approach for HD.
440 Therefore, our next objective was to assess if HTT palmitoylation levels can be
441 upregulated in various HD models using alternative approaches. To test this, we chose
442 to reduce protein depalmitoylation via the inhibition of the APT enzymes that catalyze
443 thioester hydrolysis of palmitoylated cysteine residues (**Figure 5**). We chose the well
444 characterized and membrane-permeable chiral acyl-β-lactone Palmostatin B (PalmB)
445 (IC_{50} = 5.4 nM) that inhibits the APT1 and APT2 enzymes (Dekker et al., 2010; Vujic et
446 al., 2016). PalmB has also been shown to partially inhibits the activity of FASN, PNPLA6,
447 and ABHD proteins (Lin and Conibear, 2015a).

448 The impact of PalmB treatment on mHTT palmitoylation levels in COS-7 cells
449 transiently expressing N-terminal fragments HTT_{1-548} (N548), HTT_{1-1212} (N1212) or full
450 length HTT_{1-3144} 18Q (wt) or 128Q was assessed by metabolic labelling with palmitic acid
451 alkyne followed by bioorthogonal labelling (click chemistry) (**Figure 5.A**). The PalmB
452 concentration of 15 μM was selected after testing a wide range of concentrations (0, 10,
453 15, 20 and 50 μM) in our experimental models. Palmitoylation levels of N548, N1212 and
454 full length HTT were significantly decreased in the presence of the HD mutation, with a
455 stronger effect for shorter fragments (2WA: HD mutation, $p<0.0001$ for N548 and N1212,
456 and $p=0.0002$ for full length HTT). Treatment of COS-7 cells with 15 μM PalmB for 6h
457 significantly increased the palmitoylation levels of 15Q and 128Q N548, N1212 and full

458 length HTT compared to the respective DMSO controls (2WA: PalmB effect: $p<0.0001$ for
459 N548 and full length HTT, and $p=0.0007$ for N1212). Notably, palmitoylation levels of full
460 length mHTT were restored to those of wtHTT following treatment with PalmB.

461 We next used primary cortico-striatal neuronal cultures from YAC18 and YAC128 mice to
462 evaluate the impact of PalmB treatment on HTT palmitoylation levels (**Figure 5.B**). As
463 expected, the palmitoylation level of mHTT was significantly decreased compared to
464 mouse Htt and wtHTT (2WA: HD mutation, $p<0.0001$). Treatment with PalmB significantly
465 increased human HTT palmitoylation (2WA: PalmB effect, $p=0.032$). In the YAC128
466 neuronal cultures, wt and mHTT palmitoylation was significantly increased by the PalmB
467 treatment compared to the DMSO control by approximately 20% (Bonferroni's test (Bf):
468 $p=0.041$ and $p=0.028$). In the YAC18 neuronal culture, the effect of PalmB on the
469 palmitoylation levels of mouse Htt and human wtHTT (not distinguishable with our
470 protocol) was weaker (Bf: $p=0.54$).

471 Finally, we explored the impact of PalmB treatment on HTT palmitoylation in control and
472 HD-patient derived lymphoblasts (**Figure 5.C**). Notably, treatment with PalmB
473 significantly increased HTT palmitoylation in this model (2WA: PalmB effect, $p=0.0071$),
474 rescuing mHTT palmitoylation levels to wtHTT palmitoylation level.

475 Inhibiting the activity of the APT enzymes with PalmB treatment significantly
476 increased full length HTT palmitoylation levels in immortalized cell lines, primary YAC128
477 neuronal cultures and HD patient-derived cells. Therefore, the impact of the HD mutation
478 on mHTT palmitoylation is reversible and can be modulated using small molecules.

479 **3.6. Inhibition of APTs with PalmB treatment reduces mHTT-induced cytotoxicity in**
480 **COS-7 cells and YAC128 primary neurons**

481 Our last objective was to investigate if increasing mHTT palmitoylation levels
482 through APT inhibition would impact mHTT inclusion formation and/or mHTT-induced cell
483 toxicity in an *in vitro* HD model. We measured the impact of PalmB treatment in COS-7
484 cells transfected with mutant 138Q HTT_{1-588}-YFP (138Q-N588-YFP) on the quantity of
485 insoluble mHTT inclusions by filter retardation assay (**Figure 6**). We confirmed that
486 PalmB treatment increased 138Q-N588-YFP palmitoylation level (by 30%) compared to
487 the DMSO treated control (p=0.029) (**Figure 6.A**), and that the amount of insoluble HTT
488 inclusions were significantly higher when 138Q-N588-YFP is expressed compared to
489 17Q-N588-YFP (p<0.0001) (**Figure 6.B**) consistent with a previous study (D. D. O. Martin
490 et al., 2018). Treatment with PalmB for 48h significantly decreased the formation of
491 insoluble inclusions by 20-22% (p=0.038 and 0.0065 with HTT or GFP antibodies) (**Figure**
492 **6.C**).

493 The impact of APT inhibition on cytotoxicity was measured using the LDH activity
494 assay in COS-7 cells transiently expressing 15Q or 128Q-HTT_{1-3144}. First, we confirmed
495 that the expression of full length 128Q-HTT increased cytotoxicity (relative to
496 untransfected cells) compared to 15Q-HTT (p=0.019) (**Figure 6.D**). Then, we measured
497 the impact of PalmB treatment for 6 or 24h on cytotoxicity in COS-7 expressing 128Q-
498 HTT (**Figure 6.E**). Negative cytotoxicity values correspond to a protective effect of the
499 treatment. Treatment with PalmB for 6 and 24h significantly reduced cytotoxicity in COS-
500 7 cells expressing 128Q-HTT relatively to DMSO controls (2WA: PalmB effect, p<0.0001).
501 The effect of PalmB on cytotoxicity compared to the DMSO control was the strongest at

502 a concentration of 30 μM, but was also significant at lower concentrations (Dunnett's test:
503 $p<0.05$).

504 The impact of PalmB treatment on cytotoxicity was also assessed in YAC128 cortico-
505 striatal primary neurons (**Figure 6.F**). Cytotoxicity was significantly reduced by the PalmB
506 treatment compared to neuron treated with DMSO (2WA: PalmB effect, $p=0.0014$). The
507 effect of PalmB against cytotoxicity compared to the DMSO treated control was the
508 strongest with 10 μM and 15 μM after 6 and 24h or treatment, respectively (Dunnett's
509 test: $p=0.048$ and 0.0098).

510 Altogether, the data shows that inhibiting of APTs with PalmB reduces mHTT
511 inclusion levels and mHTT-induced cytotoxicity in COS-7 cells and YAC128 cortico-
512 striatal primary neurons.

513 **4. Discussion**

514 Targeting the causative agent of HD, by lowering levels of the toxic mHTT protein,
515 is one of the therapeutic strategies for the treatment of this disease (Caron et al., 2018).
516 This can be achieved by suppressing transcription of *HTT*, reducing the synthesis of the
517 toxic protein or increasing its degradation in cells. Promising strategies to promote mHTT
518 degradation use mHTT-LC3 linker compounds (Li et al., 2019) or proteolysis-targeting
519 chimera (PROTAC) based approaches (Harding and Tong, 2018). Another approach has
520 been to target specific PTMs of HTT that are dysregulated in presence of the HD mutation
521 in order to promote neuronal survival (Aharony et al., 2015; Bowie et al., 2018; Di Pardo
522 et al., 2012; Ehrnhoefer et al., 2011; Gu et al., 2009; Kratter et al., 2016).

523 The challenge with this strategy lies in the identification of enzymes adding or
524 removing PTMs with a high specificity for HTT. Most kinases, phosphatases or caspases
525 have a large variety of substrates. Developing therapeutically relevant pharmacological
526 modulators of PTM requires that they be developed within the context of well-
527 characterized PTM-related signaling systems. However, there are still many knowledge
528 gaps regarding the role of PTM dysregulation on mHTT toxicity in human tissues that will
529 need to be addressed to develop effective therapies.

530 A potential PTM candidate is palmitoylation of HTT at cysteine 214, catalyzed by
531 HIP14 (ZDHHC17) and HIP14L (ZDHHC13) (Yanai et al., 2006). Here, we showed that
532 palmitoylation levels of HTT and various HIP14/14L substrates were reproducibly reduced
533 in a variety of HD models, including humanized HD mouse models, HD patient-derived
534 lymphoblast and isogenic hiPSCs (**Figures 1 and 3**). Palmitoylation of HTT was
535 decreased as early as 1 month of age in the HD humanized mouse model and

536 palmitoylation levels were further decreased with aging (**Figure 2**). Lowering mHTT levels
537 in the YAC128 mouse brain was not sufficient to rescue palmitoylation levels of synaptic
538 HIP14/14L substrates (**Figure 4**). Treatment of COS-7 cells, YAC128 cortico-striatal
539 neurons and in HD patient derived lymphoblast with Palm B, a small molecule that targets
540 mainly APTs 1 and 2, normalized palmitoylation of full length mHTT (**Figure 5**). Finally,
541 modulating mHTT palmitoylation was beneficial against mHTT-induced cytotoxicity
542 (**Figure 6**).

543 Our first aim was to investigate how the HD mutation impacts HTT palmitoylation
544 in multiple mouse and human HD models to address model biases and technical
545 limitations previously encountered and to obtain a more accurate representation of
546 palmitoylation dysregulation that may occur in HD patients. The palmitoylation of mHTT
547 was previously shown to be reduced by 50% in COS-7 cells expressing 15Q and 128Q
548 N548 and metabolically labelled with [^{3}H]-palmitate, and by 80% in the YAC128 HD
549 mouse brain compared to wtHTT in the YAC18 brain (a different mouse line than YAC128
550 expressing endogenous mouse 7Q-Htt and human 18Q-HTT) by IP of human HTT (Yanai
551 et al., 2006) followed by the earliest version of the ABE assay (Drisdel and Green, 2004),
552 which now has been optimized to yield higher sensitivity (Brigidi and Bamji, 2013).

553 A potential confounding factor of using the YAC128 and BACHD mouse models is the
554 presence of two endogenous mouse Htt alleles in addition to the mHTT transgene, which
555 could compensate for the effect of mHTT on HIP14 and HIP14L activity. To take this into
556 consideration, the two humanized HD mouse models, Hu97/18 and Hu128/21, which
557 harbor a mutant and a wtHTT human transgene with no mouse Htt complement, were

558 also used to investigate palmitoylation in a model that more closely models the human
559 condition. In all four mouse models of HD, mHTT palmitoylation was reproducibly and
560 consistently decreased both compared to littermate control mice and compared to the WT
561 protein within the same mouse (**Figure 1**).

562 To assess HTT palmitoylation in a more physiologically relevant system, we used
563 control and HD patient-derived lymphoblasts. We observed that palmitoylation of HTT is
564 decreased with increasing number of polyQ repeats (**Figure 3.A-D**). This is, to our
565 knowledge, the first demonstration of aberrant palmitoylation of mHTT in a HD human
566 cell model. This supports the finding that decreased palmitoylation of mHTT in the brains
567 of a variety of HD mouse models is not an artifact due to lower affinity of mouse HIP14/14L
568 (or potentially other PATs) for the human huntingtin protein, but a robust biochemical
569 phenotype. Previous studies have looked at palmitoylation dysregulation in HD models
570 with extreme polyQ lengths (>90) rarely seen in the clinic (Huang et al., 2011; Yanai et
571 al., 2006). Our results now suggest that aberrant palmitoylation of HTT occurs within a
572 range of clinically-relevant polyQ-repeat lengths found in HD patients. We also provide
573 the first evidence that mHTT palmitoylation levels are inversely correlated with polyQ
574 repeat length. The data generated in two sets of isogenic control and HD (IsoHD) hPSC
575 lines (**Figure 3.E-F**) suggests that the differences of palmitoylation level are not due to
576 additional factors such as genetic variants beside the *HTT* gene.

577 Our next objective was to investigate the earliest timepoint at which palmitoylation
578 is altered in the humanized HD mouse model, Hu128/21 (**Figure 2**). We showed that
579 palmitoylation of mHTT was decreased very early in the whole brain (at 1 month), before

580 onset of behavioural and neuropathological HD-like phenotypes (Southwell et al., 2017),
581 making it one of the earliest phenotypes observed in this model. This downregulation of
582 mHTT palmitoylation is maintained at 3, 6 and 12 months in the brain of Hu128/21.
583 Additional studies are required to determine if mHTT is hypo-palmitoylated during
584 embryonic development.

585 We report here for the first time that aging led to a decrease of both wtHTT and
586 mHTT palmitoylation. This suggests that the presence of the HD mutation has the same
587 impact as aging on HTT palmitoylation levels. The combined impact of aging and the HD
588 mutation may be additive in reducing palmitoylation levels. The relationship between
589 palmitoylation levels of proteins in aging have not been extensively investigated (Zamzow
590 et al., 2019).

591 Therapeutics that lower toxic mHTT have shown promise in preclinical studies in
592 HD rodents (Kordasiewicz et al., 2012; Southwell et al., 2018) and are currently being
593 evaluated in clinical trials for HD (NCT04120493, NCT04000594 and NCT03225833). We
594 have previously shown that reducing levels of Htt in *Htt*$^{+/-}$ mice and FVB neurons treated
595 with HTT-ASO (~95% HTT knockdown) leads to reduced palmitoylation of HIP14 and
596 HIP14 substrates such as SNAP25 and GluR1 (Huang et al., 2011). However, the impact
597 of lowering mHTT on palmitoylation of HIP14 and HIP14L substrates has not been
598 investigated. Our data from YAC128 animals treated with an ASO against mHTT at 5
599 months of age and assessed at 6 months of age (**Figure 4;** ~90% reduction of mHTT
600 levels in the whole brain) suggests that mHTT lowering for 1 month is not sufficient to
601 rescue palmitoylation alterations in HD. This suggest that specific palmitoylation-targeted

602 therapies may be necessary. Additional studies to investigate the impact of ASO treatment
603 at a younger age, or for a longer duration are needed.

604 Aberrant palmitoylation causes or contributes to a large variety of disorders such
605 as Alzheimer's disease , schizophrenia, mental retardation and Batten Disease
606 (Bhattacharyya et al., 2013; Cho and Park, 2016; Hofmann and Lu, 2014; Ko and Dixon,
607 2018). The concept of developing therapeutically relevant pharmacological modulators of
608 palmitoylation to promote or reduce palmitoylation of specific proteins has been emerging
609 over the past years (Chavda et al., 2014; Fraser et al., 2019). In this study, we observed
610 robust reduction of HTT palmitoylation in a variety of HD models. HTT is dynamically
611 palmitoylated by HIP14 and 14L and de-palmitoylated by APTs 1 and 2 (also LYPA1 and
612 2) (Lin and Conibear, 2015b; Yanai et al., 2006). We have previously shown that
613 increasing mHTT palmitoylation levels *in vitro* by overexpression of HIP14 may be
614 protective (Yanai et al., 2006), but this approach is not easily translatable *in vivo*. Inhibition
615 of APTs with the membrane-permeable chiral acyl-β-lactone PalmB (Davda and Martin,
616 2014; Dekker et al., 2010; Vujic et al., 2016) was shown to increase HTT_{1-548}
617 palmitoylation levels in COS-7 cells (Lin and Conibear, 2015b). Here, we demonstrate
618 that PalmB can be used to promote palmitoylation of full length mHTT in multiple models
619 (**Figure 5**).

620 This study serves as a proof-of-concept that mHTT palmitoylation can be
621 increased, and even normalized to wtHTT levels, using a small molecule. Furthermore,
622 we show that increasing palmitoylation of mHTT exerts beneficial effects on aggregation
623 and cytotoxicity (**Figure 6**). Further studies evaluating the impact of promoting HTT

624 palmitoylation on well characterized HD phenotypes will help elucidate the potential
625 mechanism of action leading to the observed protective effects. PalmB inhibits APT 1 and
626 2 that depalmitoylate a large variety of protein substrates, and also targets FASN,
627 PNPLA6, and ABHD proteins (Lin and Conibear, 2015a). Testing additional APT inhibitors
628 (Vujic et al., 2016) or developing new ones specifically disrupting the interaction between
629 APTs and HTT or HIP14 to evaluate the impact of promoting HTT palmitoylation in
630 preclinical models will be critical.

631 Protective effects of promoting palmitoylation of HTT and other substrates may be
632 mediated by increased mHTT clearance, or reduced proteolytic cleavage of mHTT by
633 caspase 6 (CASP6) at D586. We have indeed recently shown that CASP6 is
634 palmitoylated by HIP14, resulting in CASP6 inactivation (Lontay et al., 2020; Skotte et al.,
635 2017) which would be expected to reduce cleavage and potentially provide beneficial
636 effects.

637 **Acknowledgments & Funding**

638 The authors would like to thank Mark Wang, Xiaofan Qu and Qingwen Xia for their
639 technical support, Dr. Amirah Ali, Dr. Philip Ly, Hailey Findlay-Black, Jennifer Collins, Dr.
640 Niels Skotte, Dr. Amber Southwell and Stephanie Bortnick for their support on the project.
641 FLL was funded by a Canadian Institutes of Health Research (CIHR) Postdoctoral
642 Fellowship. NSC was funded by the Ripples of Hope Pfizer Trainee Award, a Canadian
643 Institutes for Health Research Postdoctoral Fellowship, and the Huntington Disease
644 Society of America Berman/Topper Family HD Career Development Fellowship. MES
645 was supported by a Vanier Canada Graduate Scholarship and a University of British
646 Columbia 4-Year Graduate Fellowship. MAP is Michael Smith Foundation for Health
647 Research Scholar. Project operational support for MRH provided by a CIHR Foundation
648 grant (FDN-154278) and by the CHDI Foundation.

649 **Conflict of Interest**

650 The authors have no conflict of interest to report.

651 **BIBLIOGRAPHY**

652 Aharony, I., Ehrnhoefer, D.E., Shruster, A., Qiu, X., Franciosi, S., Hayden, M.R., Offen,
653 D., 2015. A Huntingtin-based peptide inhibitor of caspase-6 provides protection
654 from mutant Huntingtin-induced motor and behavioral deficits. Hum Mol Genet
655 24, 2604–2614. https://doi.org/10.1093/hmg/ddv023
656 Aiken, C.T., Steffan, J.S., Guerrero, C.M., Khashwji, H., Lukacsovich, T., Simmons, D.,
657 Purcell, J.M., Menhaji, K., Zhu, Y.-Z., Green, K., Laferla, F., Huang, L.,
658 Thompson, L.M., Marsh, J.L., 2009. Phosphorylation of threonine 3: implications
659 for Huntingtin aggregation and neurotoxicity. J. Biol. Chem. 284, 29427–29436.
660 https://doi.org/10.1074/jbc.M109.013193
661 Atwal, R.S., Desmond, C.R., Caron, N., Maiuri, T., Xia, J., Sipione, S., Truant, R., 2011.
662 Kinase inhibitors modulate huntingtin cell localization and toxicity. Nat. Chem.
663 Biol. 7, 453–460. https://doi.org/10.1038/nchembio.582
664 Atwal, R.S., Xia, J., Pinchev, D., Taylor, J., Epand, R.M., Truant, R., 2007. Huntingtin
665 has a membrane association signal that can modulate huntingtin aggregation,
666 nuclear entry and toxicity. Hum. Mol. Genet. 16, 2600–2615.
667 https://doi.org/10.1093/hmg/ddm217
668 Bhattacharyya, R., Barren, C., Kovacs, D.M., 2013. Palmitoylation of Amyloid Precursor
669 Protein Regulates Amyloidogenic Processing in Lipid Rafts. J Neurosci 33,
670 11169–11183. https://doi.org/10.1523/JNEUROSCI.4704-12.2013
671 Bowie, L.E., Maiuri, T., Alpaugh, M., Gabriel, M., Arbez, N., Galleguillos, D., Hung,
672 C.L.K., Patel, S., Xia, J., Hertz, N.T., Ross, C.A., Litchfield, D.W., Sipione, S.,
673 Truant, R., 2018. N6-Furfuryladenine is protective in Huntington's disease
674 models by signaling huntingtin phosphorylation. PNAS 115, E7081–E7090.
675 https://doi.org/10.1073/pnas.1801772115
676 Brigidi, G.S., Bamji, S.X., 2013. Detection of protein palmitoylation in cultured
677 hippocampal neurons by immunoprecipitation and acyl-biotin exchange (ABE). J
678 Vis Exp. https://doi.org/10.3791/50031
679 Cariulo, C., Azzollini, L., Verani, M., Martufi, P., Boggio, R., Chiki, A., Deguire, S.M.,
680 Cherubini, M., Gines, S., Marsh, J.L., Conforti, P., Cattaneo, E., Santimone, I.,
681 Squitieri, F., Lashuel, H.A., Petricca, L., Caricasole, A., 2017. Phosphorylation of
682 huntingtin at residue T3 is decreased in Huntington's disease and modulates
683 mutant huntingtin protein conformation. PNAS 114, E10809–E10818.
684 https://doi.org/10.1073/pnas.1705372114
685 Cariulo, C., Verani, M., Martufi, P., Ingenito, R., Finotto, M., Deguire, S.M., Lavery, D.J.,
686 Toledo-Sherman, L., Lee, R., Doherty, E.M., Vogt, T.F., Dominguez, C., Lashuel,
687 H.A., Petricca, L., Caricasole, A., 2020. Ultrasensitive quantitative measurement
688 of huntingtin phosphorylation at residue S13. Biochem. Biophys. Res. Commun.
689 521, 549–554. https://doi.org/10.1016/j.bbrc.2019.09.097
690 Caron, N.S., Desmond, C.R., Xia, J., Truant, R., 2013. Polyglutamine domain flexibility
691 mediates the proximity between flanking sequences in huntingtin. Proceedings of
692 the National Academy of Sciences of the United States of America 110, 14610–
693 14615. https://doi.org/10.1073/pnas.1301342110
694 Caron, N.S., Dorsey, E.R., Hayden, M.R., 2018. Therapeutic approaches to Huntington
695 disease: from the bench to the clinic. Nat Rev Drug Discov 17, 729–750.
696 https://doi.org/10.1038/nrd.2018.133

697 Carroll, J.B., Warby, S.C., Southwell, A.L., Doty, C.N., Greenlee, S., Skotte, N., Hung,
698 G., Bennett, C.F., Freier, S.M., Hayden, M.R., 2011. Potent and selective
699 antisense oligonucleotides targeting single-nucleotide polymorphisms in the
700 Huntington disease gene / allele-specific silencing of mutant huntingtin. Mol Ther
701 19, 2178–2185. https://doi.org/10.1038/mt.2011.201
702 Chavda, B., Arnott, J.A., Planey, S.L., 2014. Targeting protein palmitoylation: selective
703 inhibitors and implications in disease. Expert Opin Drug Discov 9, 1005–1019.
704 https://doi.org/10.1517/17460441.2014.933802
705 Cho, E., Park, M., 2016. Palmitoylation in Alzheimer's disease and other
706 neurodegenerative diseases. Pharmacol. Res. 111, 133–151.
707 https://doi.org/10.1016/j.phrs.2016.06.008
708 Davda, D., Martin, B.R., 2014. Acyl protein thioesterase inhibitors as probes of dynamic
709 S-palmitoylation. Medchemcomm 5, 268–276.
710 https://doi.org/10.1039/C3MD00333G
711 Dekker, F.J., Rocks, O., Vartak, N., Menninger, S., Hedberg, C., Balamurugan, R.,
712 Wetzel, S., Renner, S., Gerauer, M., Schölermann, B., Rusch, M., Kramer, J.W.,
713 Rauh, D., Coates, G.W., Brunsveld, L., Bastiaens, P.I.H., Waldmann, H., 2010.
714 Small-molecule inhibition of APT1 affects Ras localization and signaling. Nat.
715 Chem. Biol. 6, 449–456. https://doi.org/10.1038/nchembio.362
716 Di Pardo, A., Maglione, V., Alpaugh, M., Horkey, M., Atwal, R.S., Sassone, J.,
717 Ciammola, A., Steffan, J.S., Fouad, K., Truant, R., Sipione, S., 2012. Ganglioside
718 GM1 induces phosphorylation of mutant huntingtin and restores normal motor
719 behavior in Huntington disease mice. Proc. Natl. Acad. Sci. U.S.A. 109, 3528–
720 3533. https://doi.org/10.1073/pnas.1114502109
721 Drisdel, R.C., Green, W.N., 2004. Labeling and quantifying sites of protein
722 palmitoylation. BioTechniques 36, 276–285.
723 Ehrnhoefer, D.E., Sutton, L., Hayden, M.R., 2011. Small changes, big impact:
724 posttranslational modifications and function of huntingtin in Huntington disease.
725 Neuroscientist 17, 475–492. https://doi.org/10.1177/1073858410390378
726 Evans, S.J.W., Douglas, I., Rawlins, M.D., Wexler, N.S., Tabrizi, S.J., Smeeth, L., 2013.
727 Prevalence of adult Huntington's disease in the UK based on diagnoses recorded
728 in general practice records. J. Neurol. Neurosurg. Psychiatry 84, 1156–1160.
729 https://doi.org/10.1136/jnnp-2012-304636
730 Fisher, E.R., Hayden, M.R., 2014. Multisource ascertainment of Huntington disease in
731 Canada: prevalence and population at risk. Mov. Disord. 29, 105–114.
732 https://doi.org/10.1002/mds.25717
733 Fraser, N.J., Howie, J., Wypijewski, K.J., Fuller, W., 2019. Therapeutic targeting of
734 protein S-acylation for the treatment of disease. Biochemical Society
735 Transactions 48, 281–290. https://doi.org/10.1042/BST20190707
736 Fukata, Y., Fukata, M., 2010. Protein palmitoylation in neuronal development and
737 synaptic plasticity. Nat. Rev. Neurosci. 11, 161–175.
738 https://doi.org/10.1038/nrn2788
739 Globa, A.K., Bamji, S.X., 2017. Protein palmitoylation in the development and plasticity
740 of neuronal connections. Curr Opin Neurobiol 45, 210–220.
741 https://doi.org/10.1016/j.conb.2017.02.016

742 Graham, R.K., Deng, Y., Slow, E.J., Haigh, B., Bissada, N., Lu, G., Pearson, J.,
743 Shehadeh, J., Bertram, L., Murphy, Z., Warby, S.C., Doty, C.N., Roy, S.,
744 Wellington, C.L., Leavitt, B.R., Raymond, L.A., Nicholson, D.W., Hayden, M.R.,
745 2006. Cleavage at the caspase-6 site is required for neuronal dysfunction and
746 degeneration due to mutant huntingtin. Cell 125, 1179–1191.
747 https://doi.org/10.1016/j.cell.2006.04.026
748 Gray, M., Shirasaki, D.I., Cepeda, C., André, V.M., Wilburn, B., Lu, X.-H., Tao, J.,
749 Yamazaki, I., Li, S.-H., Sun, Y.E., Li, X.-J., Levine, M.S., Yang, X.W., 2008. Full-
750 length human mutant huntingtin with a stable polyglutamine repeat can elicit
751 progressive and selective neuropathogenesis in BACHD mice. J. Neurosci. 28,
752 6182–6195. https://doi.org/10.1523/JNEUROSCI.0857-08.2008
753 Gu, X., Greiner, E.R., Mishra, R., Kodali, R., Osmand, A., Finkbeiner, S., Steffan, J.S.,
754 Thompson, L.M., Wetzel, R., Yang, X.W., 2009. Serines 13 and 16 are critical
755 determinants of full-length human mutant huntingtin induced disease
756 pathogenesis in HD mice. Neuron 64, 828–840.
757 https://doi.org/10.1016/j.neuron.2009.11.020
758 Harding, R.J., Tong, Y., 2018. Proteostasis in Huntington's disease: disease
759 mechanisms and therapeutic opportunities. Acta Pharmacol Sin 39, 754–769.
760 https://doi.org/10.1038/aps.2018.11
761 Hofmann, S., Lu, J.-Y., 2014. Molecular basis of infantile Batten disease: impact of
762 disordered palmitoylated protein degradation on the nervous system (466.1). The
763 FASEB Journal 28, 466.1. https://doi.org/10.1096/fasebj.28.1_supplement.466.1
764 Huang, K., Sanders, S., Singaraja, R., Orban, P., Cijsouw, T., Arstikaitis, P., Yanai, A.,
765 Hayden, M.R., El-Husseini, A., 2009. Neuronal palmitoyl acyl transferases exhibit
766 distinct substrate specificity. FASEB J. 23, 2605–2615.
767 https://doi.org/10.1096/fj.08-127399
768 Huang, K., Sanders, S.S., Kang, R., Carroll, J.B., Sutton, L., Wan, J., Singaraja, R.,
769 Young, F.B., Liu, L., El-Husseini, A., Davis, N.G., Hayden, M.R., 2011. Wild-type
770 HTT modulates the enzymatic activity of the neuronal palmitoyl transferase
771 HIP14. Hum Mol Genet 20, 3356–3365. https://doi.org/10.1093/hmg/ddr242
772 Huang, K., Yanai, A., Kang, R., Arstikaitis, P., Singaraja, R.R., Metzler, M., Mullard, A.,
773 Haigh, B., Gauthier-Campbell, C., Gutekunst, C.-A., Hayden, M.R., El-Husseini,
774 A., 2004. Huntingtin-Interacting Protein HIP14 Is a Palmitoyl Transferase
775 Involved in Palmitoylation and Trafficking of Multiple Neuronal Proteins. Neuron
776 44, 977–986. https://doi.org/10.1016/j.neuron.2004.11.027
777 Hubalkova, P., Ladislav, M., Vyklicky, V., Smejkalova, T., Krausova, B.H., Kysilov, B.,
778 Krusek, J., Naimová, Z., Korinek, M., Chodounska, H., Kudova, E., Cerny, J.,
779 Vyklicky, L., 2021. Palmitoylation Controls NMDA Receptor Function and Steroid
780 Sensitivity. J. Neurosci. 41, 2119–2134.
781 https://doi.org/10.1523/JNEUROSCI.2654-20.2021
782 Humbert, S., Bryson, E.A., Cordelières, F.P., Connors, N.C., Datta, S.R., Finkbeiner, S.,
783 Greenberg, M.E., Saudou, F., 2002. The IGF-1/Akt pathway is neuroprotective in
784 Huntington's disease and involves Huntingtin phosphorylation by Akt. Dev. Cell
785 2, 831–837.
786 Jeong, H., Then, F., Melia, T.J., Mazzulli, J.R., Cui, L., Savas, J.N., Voisine, C.,
787 Paganetti, P., Tanese, N., Hart, A.C., Yamamoto, A., Krainc, D., 2009.

788 Acetylation Targets Mutant Huntingtin to Autophagosomes for Degradation. Cell
789 137, 60–72. https://doi.org/10.1016/j.cell.2009.03.018
790 Kalchman, M.A., Graham, R.K., Xia, G., Koide, H.B., Hodgson, J.G., Graham, K.C.,
791 Goldberg, Y.P., Gietz, R.D., Pickart, C.M., Hayden, M.R., 1996. Huntingtin is
792 ubiquitinated and interacts with a specific ubiquitin-conjugating enzyme. J. Biol.
793 Chem. 271, 19385–19394. https://doi.org/10.1074/jbc.271.32.19385
794 Kalchman, M.A., Koide, H.B., McCutcheon, K., Graham, R.K., Nichol, K., Nishiyama, K.,
795 Kazemi-Esfarjani, P., Lynn, F.C., Wellington, C., Metzler, M., Goldberg, Y.P.,
796 Kanazawa, I., Gietz, R.D., Hayden, M.R., 1997. HIP1 , a human homologue of S.
797 cerevisiae Sla2p , interacts with membrane-associated huntingtin in the brain.
798 Nature Genetics 16, 44–53. https://doi.org/10.1038/ng0597-44
799 Ko, P., Dixon, S.J., 2018. Protein palmitoylation and cancer. EMBO Rep 19.
800 https://doi.org/10.15252/embr.201846666
801 Kordasiewicz, H.B., Stanek, L.M., Wancewicz, E.V., Mazur, C., McAlonis, M.M., Pytel,
802 K.A., Artates, J.W., Weiss, A., Cheng, S.H., Shihabuddin, L.S., Hung, G.,
803 Bennett, C.F., Cleveland, D.W., 2012. Sustained therapeutic reversal of
804 Huntington's disease by transient repression of huntingtin synthesis. Neuron 74,
805 1031–1044. https://doi.org/10.1016/j.neuron.2012.05.009
806 Kratter, I.H., Zahed, H., Lau, A., Tsvetkov, A.S., Daub, A.C., Weiberth, K.F., Gu, X.,
807 Saudou, F., Humbert, S., Yang, X.W., Osmand, A., Steffan, J.S., Masliah, E.,
808 Finkbeiner, S., 2016. Serine 421 regulates mutant huntingtin toxicity and
809 clearance in mice. J Clin Invest 126, 3585–3597.
810 https://doi.org/10.1172/JCI80339
811 Li, Z., Wang, C., Wang, Z., Zhu, C., Li, J., Sha, T., Ma, L., Gao, C., Yang, Y., Sun, Y.,
812 Wang, J., Sun, X., Lu, C., Difiglia, M., Mei, Y., Ding, C., Luo, S., Dang, Y., Ding,
813 Y., Fei, Y., Lu, B., 2019. Allele-selective lowering of mutant HTT protein by HTT-
814 LC3 linker compounds. Nature 575, 203–209. https://doi.org/10.1038/s41586-
815 019-1722-1
816 Lin, D.T.S., Conibear, E., 2015a. ABHD17 proteins are novel protein depalmitoylases
817 that regulate N-Ras palmitate turnover and subcellular localization. eLife 4,
818 e11306. https://doi.org/10.7554/eLife.11306
819 Lin, D.T.S., Conibear, E., 2015b. ABHD17 proteins are novel protein depalmitoylases
820 that regulate N-Ras palmitate turnover and subcellular localization. Elife 4,
821 e11306. https://doi.org/10.7554/eLife.11306
822 Lontay, B., Kiss, A., Virág, L., Tar, K., 2020. How Do Post-Translational Modifications
823 Influence the Pathomechanistic Landscape of Huntington's Disease? A
824 Comprehensive Review. International Journal of Molecular Sciences 21, 4282.
825 https://doi.org/10.3390/ijms21124282
826 Maiuri, T., Mocle, A.J., Hung, C.L., Xia, J., van Roon-Mom, W.M.C., Truant, R., 2017.
827 Huntingtin is a scaffolding protein in the ATM oxidative DNA damage response
828 complex. Hum. Mol. Genet. 26, 395–406. https://doi.org/10.1093/hmg/ddw395
829 Martin, D.D.O., Heit, R.J., Yap, M.C., Davidson, M.W., Hayden, M.R., Berthiaume, L.G.,
830 2014. Identification of a post-translationally myristoylated autophagy-inducing
831 domain released by caspase cleavage of huntingtin. Hum. Mol. Genet. 23, 3166–
832 3179. https://doi.org/10.1093/hmg/ddu027

833 Martin, D. D. O., Kay, C., Collins, J.A., Nguyen, Y.T., Slama, R.A., Hayden, M.R., 2018.
834 A human huntingtin SNP alters post-translational modification and pathogenic
835 proteolysis of the protein causing Huntington disease. Sci Rep 8, 8096.
836 https://doi.org/10.1038/s41598-018-25903-w
837 Martin, Dale D. O., Schmidt, M.E., Nguyen, Y.T., Lazic, N., Hayden, M.R., 2018.
838 Identification of a novel caspase cleavage site in huntingtin that regulates mutant
839 huntingtin clearance. The FASEB Journal 33, 3190–3197.
840 https://doi.org/10.1096/fj.201701510RRR
841 Matt, L., Kim, K., Chowdhury, D., Hell, J.W., 2019. Role of Palmitoylation of
842 Postsynaptic Proteins in Promoting Synaptic Plasticity. Front. Mol. Neurosci. 12.
843 https://doi.org/10.3389/fnmol.2019.00008
844 Mukai, J., Dhilla, A., Drew, L.J., Stark, K.L., Cao, L., MacDermott, A.B., Karayiorgou, M.,
845 Gogos, J.A., 2008. Palmitoylation-dependent neurodevelopmental deficits in a
846 mouse model of 22q11 microdeletion. Nature Neuroscience 11, 1302–1310.
847 https://doi.org/10.1038/nn.2204
848 Myers, R.H., 2004. Huntington's disease genetics. NeuroRx 1, 255–262.
849 https://doi.org/10.1602/neurorx.1.2.255
850 Ochaba, J., Lukacsovich, T., Csikos, G., Zheng, S., Margulis, J., Salazar, L., Mao, K.,
851 Lau, A.L., Yeung, S.Y., Humbert, S., Saudou, F., Klionsky, D.J., Finkbeiner, S.,
852 Zeitlin, S.O., Marsh, J.L., Housman, D.E., Thompson, L.M., Steffan, J.S., 2014.
853 Potential function for the Huntingtin protein as a scaffold for selective autophagy.
854 Proc. Natl. Acad. Sci. U.S.A. 111, 16889–16894.
855 https://doi.org/10.1073/pnas.1420103111
856 Ooi, J., Langley, S.R., Xu, X., Utami, K.H., Sim, B., Huang, Y., Harmston, N.P., Tay,
857 Y.L., Ziaei, A., Zeng, R., Low, D., Aminkeng, F., Sobota, R.M., Ginhoux, F.,
858 Petretto, E., Pouladi, M.A., 2019. Unbiased Profiling of Isogenic Huntington
859 Disease hPSC-Derived CNS and Peripheral Cells Reveals Strong Cell-Type
860 Specificity of CAG Length Effects. Cell Rep 26, 2494-2508.e7.
861 https://doi.org/10.1016/j.celrep.2019.02.008
862 Sanders, S.S., Hou, J., Sutton, L.M., Garside, V.C., Mui, K.K.N., Singaraja, R.R.,
863 Hayden, M.R., Hoodless, P.A., 2015a. Huntingtin interacting proteins 14 and 14-
864 like are required for chorioallantoic fusion during early placental development.
865 Developmental Biology 397, 257–266.
866 https://doi.org/10.1016/j.ydbio.2014.11.018
867 Sanders, S.S., Martin, D.D.O., Butland, S.L., Lavallée-Adam, M., Calzolari, D., Kay, C.,
868 Iii, J.R.Y., Hayden, M.R., 2015b. Curation of the Mammalian Palmitoylome
869 Indicates a Pivotal Role for Palmitoylation in Diseases and Disorders of the
870 Nervous System and Cancers. PLOS Computational Biology 11, e1004405.
871 https://doi.org/10.1371/journal.pcbi.1004405
872 Sanders, S.S., Parsons, M.P., Mui, K.K.N., Southwell, A.L., Franciosi, S., Cheung, D.,
873 Waltl, S., Raymond, L.A., Hayden, M.R., 2016. Sudden death due to paralysis
874 and synaptic and behavioral deficits when Hip14/Zdhhc17 is deleted in adult
875 mice. BMC Biol. 14, 108. https://doi.org/10.1186/s12915-016-0333-7
876 Saudou, F., Humbert, S., 2016. The Biology of Huntingtin. Neuron 89, 910–926.
877 https://doi.org/10.1016/j.neuron.2016.02.003

878 Schilling, B., Gafni, J., Torcassi, C., Cong, X., Row, R.H., LaFevre-Bernt, M.A., Cusack,
879 M.P., Ratovitski, T., Hirschhorn, R., Ross, C.A., Gibson, B.W., Ellerby, L.M.,
880 2006. Huntingtin phosphorylation sites mapped by mass spectrometry.
881 Modulation of cleavage and toxicity. J. Biol. Chem. 281, 23686–23697.
882 https://doi.org/10.1074/jbc.M513507200
883 Schmidt, M.E., Caron, N.S., Aly, A.E., Lemarié, F.L., Dal Cengio, L., Ko, Y., Lazic, N.,
884 Anderson, L., Nguyen, B., Raymond, L.A., Hayden, M.R., 2020. DAPK1
885 Promotes Extrasynaptic GluN2B Phosphorylation and Striatal Spine Instability in
886 the YAC128 Mouse Model of Huntington Disease. Front. Cell. Neurosci. 14.
887 https://doi.org/10.3389/fncel.2020.590569
888 Singaraja, R.R., Huang, K., Sanders, S.S., Milnerwood, A.J., Hines, R., Lerch, J.P.,
889 Franciosi, S., Drisdel, R.C., Vaid, K., Young, F.B., Doty, C., Wan, J., Bissada, N.,
890 Henkelman, R.M., Green, W.N., Davis, N.G., Raymond, L.A., Hayden, M.R.,
891 2011. Altered palmitoylation and neuropathological deficits in mice lacking
892 HIP14. Hum. Mol. Genet. 20, 3899–3909. https://doi.org/10.1093/hmg/ddr308
893 Skotte, N.H., Sanders, S.S., Singaraja, R.R., Ehrnhoefer, D.E., Vaid, K., Qiu, X.,
894 Kannan, S., Verma, C., Hayden, M.R., 2017. Palmitoylation of caspase-6 by
895 HIP14 regulates its activation. Cell Death & Differentiation 24, 433–444.
896 https://doi.org/10.1038/cdd.2016.139
897 Slow, E.J., van Raamsdonk, J., Rogers, D., Coleman, S.H., Graham, R.K., Deng, Y.,
898 Oh, R., Bissada, N., Hossain, S.M., Yang, Y.-Z., Li, X.-J., Simpson, E.M.,
899 Gutekunst, C.-A., Leavitt, B.R., Hayden, M.R., 2003. Selective striatal neuronal
900 loss in a YAC128 mouse model of Huntington disease. Hum Mol Genet 12,
901 1555–1567. https://doi.org/10.1093/hmg/ddg169
902 Smotrys, J.E., Linder, M.E., 2004. Palmitoylation of Intracellular Signaling Proteins:
903 Regulation and Function. Annual Review of Biochemistry 73, 559–587.
904 https://doi.org/10.1146/annurev.biochem.73.011303.073954
905 Southwell, A.L., Kordasiewicz, H.B., Langbehn, D., Skotte, N.H., Parsons, M.P.,
906 Villanueva, E.B., Caron, N.S., Østergaard, M.E., Anderson, L.M., Xie, Y., Cengio,
907 L.D., Findlay-Black, H., Doty, C.N., Fitsimmons, B., Swayze, E.E., Seth, P.P.,
908 Raymond, L.A., Frank Bennett, C., Hayden, M.R., 2018. Huntingtin suppression
909 restores cognitive function in a mouse model of Huntington's disease. Sci Transl
910 Med 10. https://doi.org/10.1126/scitranslmed.aar3959
911 Southwell, A.L., Skotte, N.H., Villanueva, E.B., Østergaard, M.E., Gu, X., Kordasiewicz,
912 H.B., Kay, C., Cheung, D., Xie, Y., Waltl, S., Dal Cengio, L., Findlay-Black, H.,
913 Doty, C.N., Petoukhov, E., Iworima, D., Slama, R., Ooi, J., Pouladi, M.A., Yang,
914 X.W., Swayze, E.E., Seth, P.P., Hayden, M.R., 2017. A novel humanized mouse
915 model of Huntington disease for preclinical development of therapeutics targeting
916 mutant huntingtin alleles. Hum. Mol. Genet. 26, 1115–1132.
917 https://doi.org/10.1093/hmg/ddx021
918 Southwell, A.L., Smith, S.E.P., Davis, T.R., Caron, N.S., Villanueva, E.B., Xie, Y.,
919 Collins, J.A., Ye, M.L., Sturrock, A., Leavitt, B.R., Schrum, A.G., Hayden, M.R.,
920 2015. Ultrasensitive measurement of huntingtin protein in cerebrospinal fluid
921 demonstrates increase with Huntington disease stage and decrease following
922 brain huntingtin suppression. Sci Rep 5, 12166.
923 https://doi.org/10.1038/srep12166

924 Southwell, A.L., Warby, S.C., Carroll, J.B., Doty, C.N., Skotte, N.H., Zhang, W.,
925 Villanueva, E.B., Kovalik, V., Xie, Y., Pouladi, M.A., Collins, J.A., Yang, X.W.,
926 Franciosi, S., Hayden, M.R., 2013. A fully humanized transgenic mouse model of
927 Huntington disease. Hum. Mol. Genet. 22, 18–34.
928 https://doi.org/10.1093/hmg/dds397
929 Steffan, J.S., Agrawal, N., Pallos, J., Rockabrand, E., Trotman, L.C., Slepko, N., Illes,
930 K., Lukacsovich, T., Zhu, Y.-Z., Cattaneo, E., Pandolfi, P.P., Thompson, L.M.,
931 Marsh, J.L., 2004. SUMO modification of Huntingtin and Huntington's disease
932 pathology. Science 304, 100–104. https://doi.org/10.1126/science.1092194
933 Sutton, L.M., Sanders, S.S., Butland, S.L., Singaraja, R.R., Franciosi, S., Southwell,
934 A.L., Doty, C.N., Schmidt, M.E., Mui, K.K.N., Kovalik, V., Young, F.B., Zhang, W.,
935 Hayden, M.R., 2013. Hip14l-deficient mice develop neuropathological and
936 behavioural features of Huntington disease. Hum. Mol. Genet. 22, 452–465.
937 https://doi.org/10.1093/hmg/dds441
938 Vujic, I., Sanlorenzo, M., Esteve-Puig, R., Vujic, M., Kwong, A., Tsumura, A., Murphy,
939 R., Moy, A., Posch, C., Monshi, B., Rappersberger, K., Ortiz-Urda, S., 2016. Acyl
940 protein thioesterase 1 and 2 (APT-1, APT-2) inhibitors palmostatin B, ML348 and
941 ML349 have different effects on NRAS mutant melanoma cells. Oncotarget 7,
942 7297–7306. https://doi.org/10.18632/oncotarget.6907
943 Wanker, E.E., Scherzinger, E., Heiser, V., Sittler, A., Eickhoff, H., Lehrach, H., 1999.
944 Membrane filter assay for detection of amyloid-like polyglutamine-containing
945 protein aggregates. Meth. Enzymol. 309, 375–386.
946 Warby, S.C., Chan, E.Y., Metzler, M., Gan, L., Singaraja, R.R., Crocker, S.F.,
947 Robertson, H.A., Hayden, M.R., 2005. Huntingtin phosphorylation on serine 421
948 is significantly reduced in the striatum and by polyglutamine expansion in vivo.
949 Hum Mol Genet 14, 1569–1577. https://doi.org/10.1093/hmg/ddi165
950 Xu, X., Ng, B., Sim, B., Radulescu, C.I., Yusof, N.A.B.M., Goh, W.I., Lin, S., Lim, J.S.Y.,
951 Cha, Y., Kusko, R., Kay, C., Ratovitski, T., Ross, C., Hayden, M.R., Wright, G.,
952 Pouladi, M.A., 2020. pS421 huntingtin modulates mitochondrial phenotypes and
953 confers neuroprotection in an HD hiPSC model. Cell Death & Disease 11, 1–12.
954 https://doi.org/10.1038/s41419-020-02983-z
955 Xu, X., Tay, Y., Sim, B., Yoon, S.-I., Huang, Y., Ooi, J., Utami, K.H., Ziaei, A., Ng, B.,
956 Radulescu, C., Low, D., Ng, A.Y.J., Loh, M., Venkatesh, B., Ginhoux, F.,
957 Augustine, G.J., Pouladi, M.A., 2017. Reversal of Phenotypic Abnormalities by
958 CRISPR/Cas9-Mediated Gene Correction in Huntington Disease Patient-Derived
959 Induced Pluripotent Stem Cells. Stem Cell Reports 8, 619–633.
960 https://doi.org/10.1016/j.stemcr.2017.01.022
961 Yanai, A., Huang, K., Kang, R., Singaraja, R.R., Arstikaitis, P., Gan, L., Orban, P.C.,
962 Mullard, A., Cowan, C.M., Raymond, L.A., Drisdel, R.C., Green, W.N.,
963 Ravikumar, B., Rubinsztein, D.C., El-Husseini, A., Hayden, M.R., 2006.
964 Palmitoylation of huntingtin by HIP14 is essential for its trafficking and function.
965 Nat. Neurosci. 9, 824–831. https://doi.org/10.1038/nn1702
966 Yap, M.C., Kostiuk, M.A., Martin, D.D.O., Perinpanayagam, M.A., Hak, P.G., Siddam,
967 A., Majjigapu, J.R., Rajaiah, G., Keller, B.O., Prescher, J.A., Wu, P., Bertozzi,
968 C.R., Falck, J.R., Berthiaume, L.G., 2010. Rapid and selective detection of fatty

969 acylated proteins using omega-alkynyl-fatty acids and click chemistry. J. Lipid
970 Res. 51, 1566–1580. https://doi.org/10.1194/jlr.D002790
971 Zamzow, D.R., Elias, V., Acosta, V.A., Escobedo, E., Magnusson, K.R., 2019. Higher
972 Levels of Protein Palmitoylation in the Frontal Cortex across Aging Were
973 Associated with Reference Memory and Executive Function Declines. eNeuro 6.
974 https://doi.org/10.1523/ENEURO.0310-18.2019

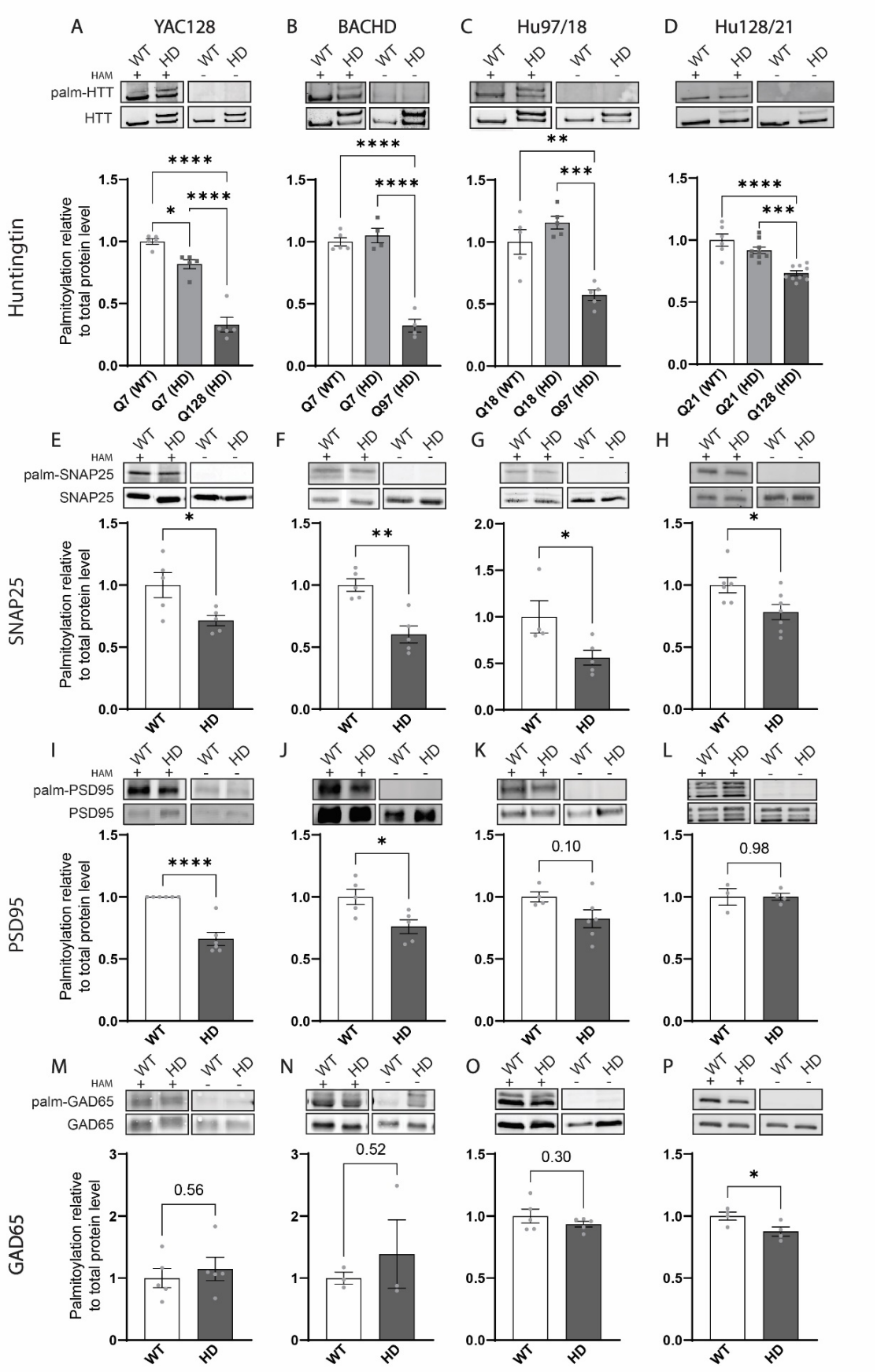
A
YAC128
B
BACHD
C
Hu97/18
D
Hu128/21
WT
HD
HAM
palm-HTT
HTT
Huntingtin
Palmitoylation relative to total protein level
Q7 (WT)
Q7 (HD)
Q128 (HD)
Q97 (HD)
Q18 (WT)
Q18 (HD)
Q21 (WT)
Q21 (HD)
E
F
G
H
palm-SNAP25
SNAP25
SNAP25
I
J
K
L
palm-PSD95
PSD95
PSD95
0.10
0.98
M
N
O
P
palm-GAD65
GAD65
GAD65
0.56
0.52
0.30

975

976 **<u>Figure 1</u> – Palmitoylation levels of mutant HTT, SNAP25, PSD95 and GAD65 are**
977 **reduced in the BACHD, and humanized Hu97/18 and Hu128/21 mouse models of**
978 **HD.**

979 Brain lysates from 6-month-old YAC128 and littermate controls (WT), BACHD and WT,
980 humanized Hu97/18 and Hu18/18, Hu128/21 and Hu21/21 mice were subjected to the
981 ABE assay. The palmitoylation signal (HAM+) is shown in the top panels for each mouse
982 line and protein, and the total protein immunoprecipitated is presented in the
983 corresponding bottom panel. The negative control (HAM-) treatment is displayed on the
984 right of each set of blots. In the huntingtin (HTT) blots (**A-D**), the lower band corresponds
985 to Htt or wtHTT, and the upper band to mHTT. The palmitoylation levels for HTT (**A-D**),
986 SNAP25 (**E-H**), PSD95 (**I-L**) and GAD65 (**M-P**) were calculated as a ratio of palmitoylation
987 over total protein signal. Mutant HTT was quantified separately from Htt or wtHTT and is
988 represented by dark grey bars on the graphs, while Htt/wtHTT from the same HD brain is
989 in light grey.

990 <u>Statistical analysis</u>: 1-way ANOVA: (**A**) YAC128 and (**B**) BACHD, $p<0.0001$; (**C**) Hu97/18,
991 $p=0.0002$; (**D**) Hu128/21, $p=0.0013$. Stars indicate Tukey's multiple comparisons test
992 results. Student's T-test: (**E-P**) results are indicated by stars or p-values on the graphs.

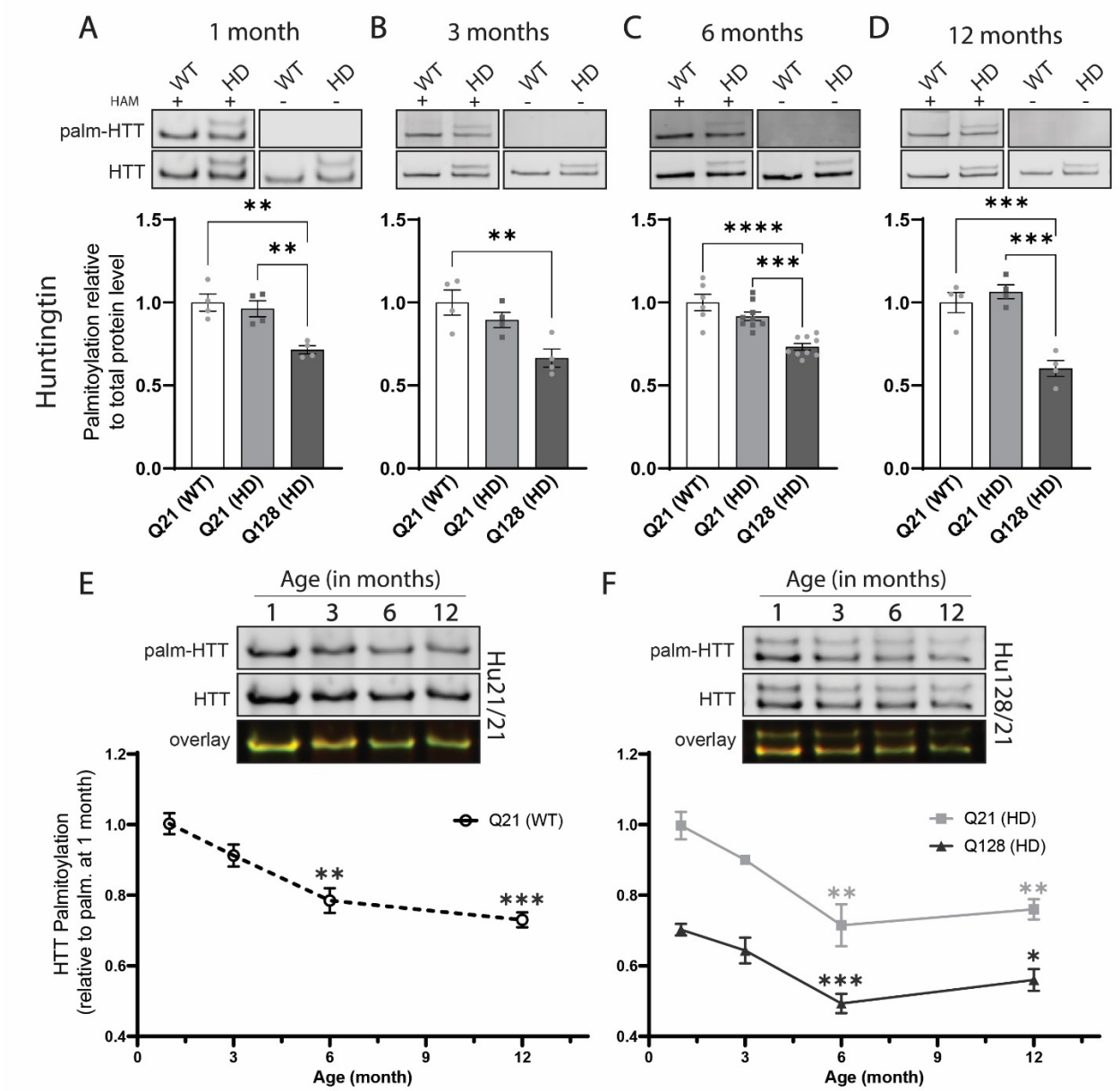

<u>Figure 2</u> - Palmitoylation of mutant HTT is decreased early in the brain of the humanized Hu128/21 mouse model of HD.

HTT palmitoylation at (**A**) 1, (**B**) 3, (**C**) 6 and (**D**) 12 months measured using the ABE assay in brain lysates from Hu21/21 (WT) and Hu128/21 (HD) mice. The palmitoylation signal (HAM+) is shown in the top panels for each time point, and the total protein immunoprecipitated is presented in the corresponding bottom panel. The negative control (HAM-) treatment is displayed on the right of each set of blots. Wildtype wtHTT (Q21) is the lower band and mHTT (Q128) the upper one. The quantification of 4-9 mice of each genotype is shown and was calculated as a ratio of HTT palmitoylation signal over total HTT and expressed relatively to wtHTT in the Hu21/21 brain. In the Hu128/21 brain, mHTT was quantified separately from wtHTT and is represented by dark grey bars while wtHTT from the same HD mice is represented by light bars.

1006 Effect of aging (1, 3, 6 and 12 months) on the palmitoylation levels of wt and mHTT in
1007 lysates from Hu21/21 (**E**) and Hu128/21 (**F**) brains. Total brain lysates at different ages
1008 were subjected to the ABE assay and run on the same gel for each genotype (n=3-4).
1009 Overlay of both channel (palm-HTT in red and total HTT in green) are displayed in the
1010 bottom panels. Palmitoylation levels of wt and mHTT brain are expressed relatively to
1011 wtHTT palmitoylation at 1 month.

1012 Statistical analysis: 1-way ANOVA: (**A**) p=0.0022; (**B**) p=0.0094; (**C**) p<0.0001; (**D**)
1013 p=0.0002. Stars indicate Tukey's multiple comparisons test results. (**E**) 1-way ANOVA:
1014 p=0.0022. Stars indicate Dunnett's test results compared to 1 month. (**F**) 2-way ANOVA:
1015 interaction, p=0.58; age and allele effect, p<0.0001. Stars indicate Dunnett's test results
1016 compared to wtHTT (Q21) or mHTT (Q128) at 1 month, and therefore only show the effect
1017 of age and not the effect of the HD mutation.

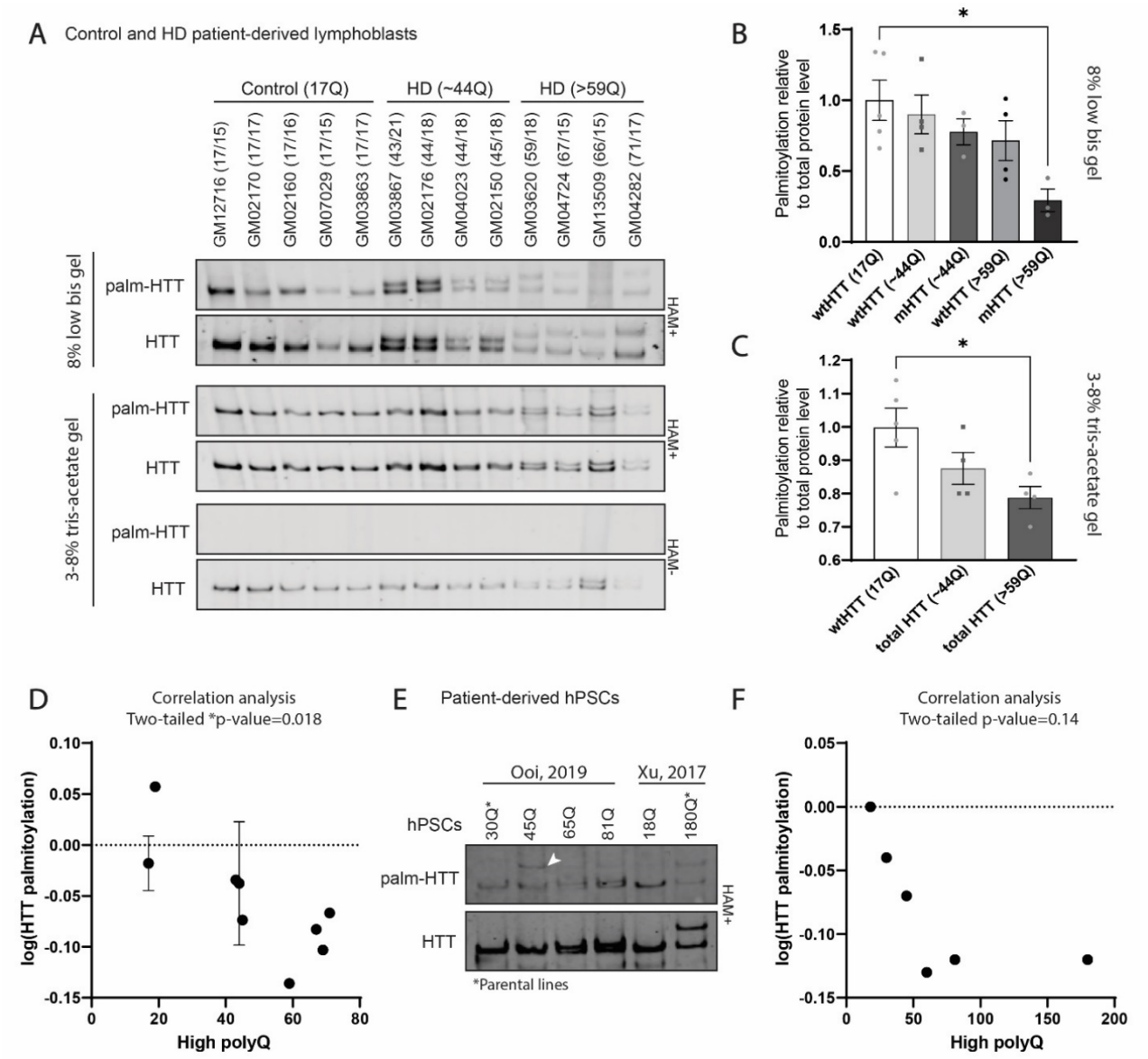

<u>Figure 3</u> - HTT palmitoylation levels decrease with increasing polyQ tract length in human lymphoblasts.

(**A**) HTT (wt and mHTT) palmitoylation levels in control and HD-patient derived lymphoblasts with increasing polyQ tract length (17 to 71). Proteins were resolved using 8% low bis or 3-8% tris-acetate gels. Palmitoylation is shown in the top panels (HAM+), and the total protein immunoprecipitated with anti-HTT (D7F7) antibodies are shown in the corresponding bottom panels. The negative control (HAM-) is shown below. Each lane corresponds to a lymphoblastoid line from a control or HD patients, and represents a biological replicate (n=4-5 for each group).

(**B**) Quantification of wt or mHTT palmitoylation levels in control and HD lymphoblasts in the control (17Q), HD (~44Q) and HD (>59Q) groups after protein separation using 8%

1032 low bis gel. The quantification is shown and is calculated as a ratio of HTT palmitoylation
1033 signal over total HTT protein and expressed relatively to wtHTT palmitoylation in the
1034 control group (17Q).
1035 (**C**) Quantification of HTT (wt and mHTT together) global palmitoylation levels measured
1036 in control (17Q), HD (~44Q) and HD (>59Q) lymphoblasts. Global palmitoylation levels of
1037 HTT was calculated as a ratio of wt and mHTT palmitoylation signal over total wt and
1038 mHTT protein and expressed relatively to wtHTT in the control (17Q) group. Mutant HTT
1039 was quantified with wtHTT, as it is challenging to resolve full length HTT alleles with small
1040 ΔQs with commonly used 3-8% tris-acetate gel.

1041 (**D**) Exponential relationship between HTT global palmitoylation levels and the polyQ tract
1042 length (high polyQ) in lymphoblasts.

1043 (**E**) HTT (wt and mutant) palmitoylation levels in HD hPSCs and isogenic controls (Ooi et
1044 al., 2019; Xu et al., 2017) with increasing polyQ tract length (18 to 180). Proteins were
1045 resolved using 3-8% tris-acetate gels. The white arrowhead indicates an unidentified
1046 band only detected with streptavidin. The hPSC parental lines used to generate HD or
1047 control hPSC lines are annotated with an asterisk.

1048 (**F**) Exponential relationship between HTT global palmitoylation level and the polyQ tract
1049 length (high polyQ) in hPSCs.

1050 Statistical analysis: 1-way ANOVA: (**B**) p=0.027; (**C**) p=0.037. Stars indicate Tukey's
1051 multiple comparisons test results. (**D**) Variance explained by polyQ tract length, R^2=0.57.
1052 Pearson r=-0.75; p=0.018. (**F**) Variance explained by polyQ tract length, R^2=0.43. Pearson
1053 r=-0.65; p=0.15.

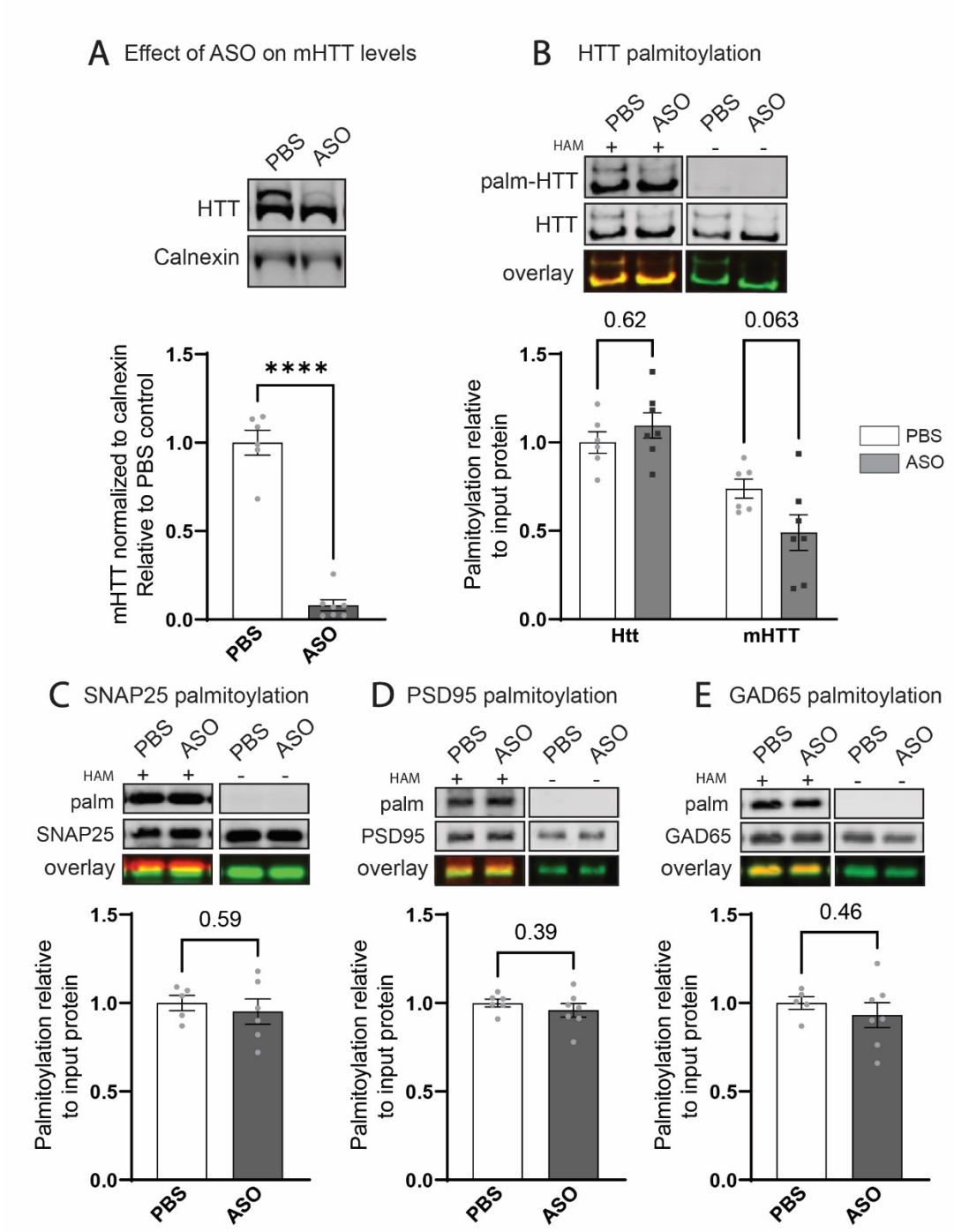

<u>Figure 4</u> – ASO-mediated mHTT lowering does not rescue aberrant palmitoylation of HIP14/HIP14L synaptic substrates in the brain of the YAC128 mouse model.

Five-month-old YAC128 mice received intracerebroventricular (ICV) injection of either PBS (n=6) or an ASO targeting human HTT (HTT-ASO; n=7), and brains were collected 1 month later.

(**A**) Protein from brain lysates were separated using 3-8% tris-acetate gradient gel and probed with HTT (MAB2166) and calnexin antibodies. HTT levels were quantified by densitometry and normalized to calnexin, and relative levels of mHTT are shown.

1063 Palmitoylation of HTT (**B**), SNAP25 (**C**), PSD95 (**D**) and GAD65 (**E**) was measured using
1064 the ABE assay. The palmitoylation signal (HAM+) is shown in the top panels for each
1065 protein, and the total protein immunoprecipitated is presented in the panels below. The
1066 negative control (HAM-) is displayed on the right of each set of blots. Overlay of both
1067 channel (palmitoylated protein in red and total protein in green) are displayed in the
1068 bottom panels. In the HTT blots (**B**), the lower band corresponds to mouse Htt, and the
1069 upper band to mHTT. The palmitoylation levels were calculated as a ratio of palmitoylation
1070 over total protein signal.

1071 Statistical analysis: (**B**) 2-way ANOVA: interaction, $p=0.059$; allele, $p<0.0001$, ASO
1072 treatment, $p=0.48$. Stars indicate Tukey's multiple comparisons test results between PBS
1073 and ASO groups. Student's T-test: (**A**, **C**, **D**, **E**) results are indicated by p-values or stars
1074 on the graphs.

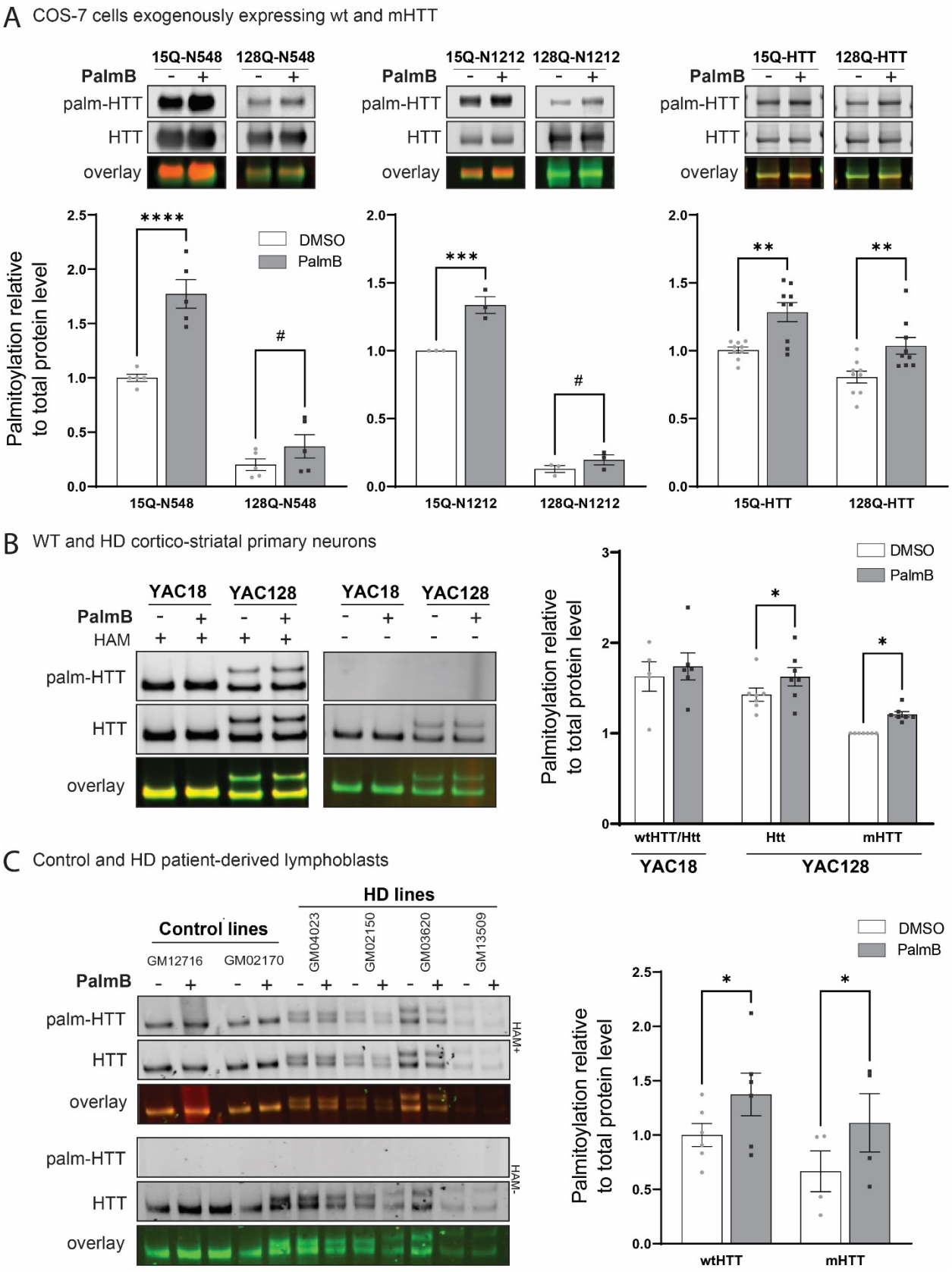
A COS-7 cells exogenously expressing wt and mHTT
15Q-N548
128Q-N548
15Q-N1212
128Q-N1212
15Q-HTT
128Q-HTT
PalmB
palm-HTT
HTT
overlay
DMSO
PalmB
Palmitoylation relative to total protein level
B WT and HD cortico-striatal primary neurons
YAC18
YAC128
HAM
wtHTT/Htt
Htt
mHTT
C Control and HD patient-derived lymphoblasts
Control lines
HD lines
GM12716
GM02170
GM04023
GM02150
GM03620
GM13509
HAM+
HAM-
wtHTT
mHTT

1076 **<u>Figure 5</u> - Inhibition of APTs with Palmostatin B increases palmitoylation level of**
1077 **HTT in COS-7 cells, YAC128 primary neurons and HD-patient derived lymphoblasts**.

1078 (**A**) COS-7 cells were transfected with the N-terminal fragments HTT_{1-548} (N548), HTT_{1-}
1079 $_{1212}$ (N1212) and full length wt (15Q) or mutant (128Q) HTT_{1-3144} constructs. Cells were
1080 treated with DMSO or 15 μM PalmB for 6h while concurrently labelled with 100 μM alkyne-
1081 palmitate. Bio-orthogonal click chemistry of alkyne-palmitate was performed on lysates
1082 immunoprecipitated with anti-HTT (MAB2166) antibodies. Palmitoylated and total HTT
1083 were detected by immunoblots using streptavidin and anti-HTT (HD46) antibodies,
1084 respectively. Overlay of both channel (palm in red and total protein in green) are displayed
1085 in the bottom panels. Palmitoylation was calculated as a ratio of palmitoylation signal over
1086 total HTT protein and are expressed relative to wtHTT palmitoylation in the DMSO control
1087 group.

1088 (**B**) YAC18 and YAC128 cortico-striatal primary neurons were treated at DIV10 with
1089 DMSO or 15 μM PalmB for 6h. Cell lysates were subjected to ABE assay to measure
1090 palmitoylated HTT. HTT was immunoprecipitated with anti-HTT (MAB2166) antibodies
1091 and detected with D7F7 for Htt (mouse) or HTT (human) and streptavidin for palmitoylated
1092 protein. HTT palmitoylation level was calculated as a ratio of palmitoylation signal over
1093 total HTT protein and expressed relative to mHTT palmitoylation in the DMSO control
1094 group.

1095 (**C**) Control and HD-patient derived lymphoblastoid lines were treated at with DMSO or
1096 10 μM PalmB for 4h, and lysates were subjected to the ABE assay. HTT was
1097 immunoprecipitated with anti-HTT (MAB2166) antibodies and detected with D7F7 for total
1098 HTT and streptavidin for palmitoylated HTT. HTT palmitoylation level was calculated as a
1099 ratio of palmitoylation signal over total HTT protein and expressed relative to wtHTT
1100 palmitoylation level in the DMSO treated control group.

1101 <u>Statistical analysis</u>: 2-way ANOVA: (**A**) N548, interaction, $p=0.0042$; HD mutation,
1102 $p<0.0001$; PalmB, <0.0001. N1212, interaction, $p=0.0075$; HD mutation, $p<0.0001$;
1103 PalmB, $p=0.0007$. Full length HTT, interaction, $p=0.65$; HD mutation, $p=0.0002$; PalmB,
1104 $p<0.0001$. (**B**) Interaction, $p=0.86$; HD mutation, $p<0.0001$; PalmB, $p=0.0320$. (**C**)
1105 Interaction, $p=0.90$; HD mutation, $p=0.43$; PalmB, $p=0.0071$. Stars indicate Bonferroni's
1106 multiple comparisons test results and hashtag t-test results.

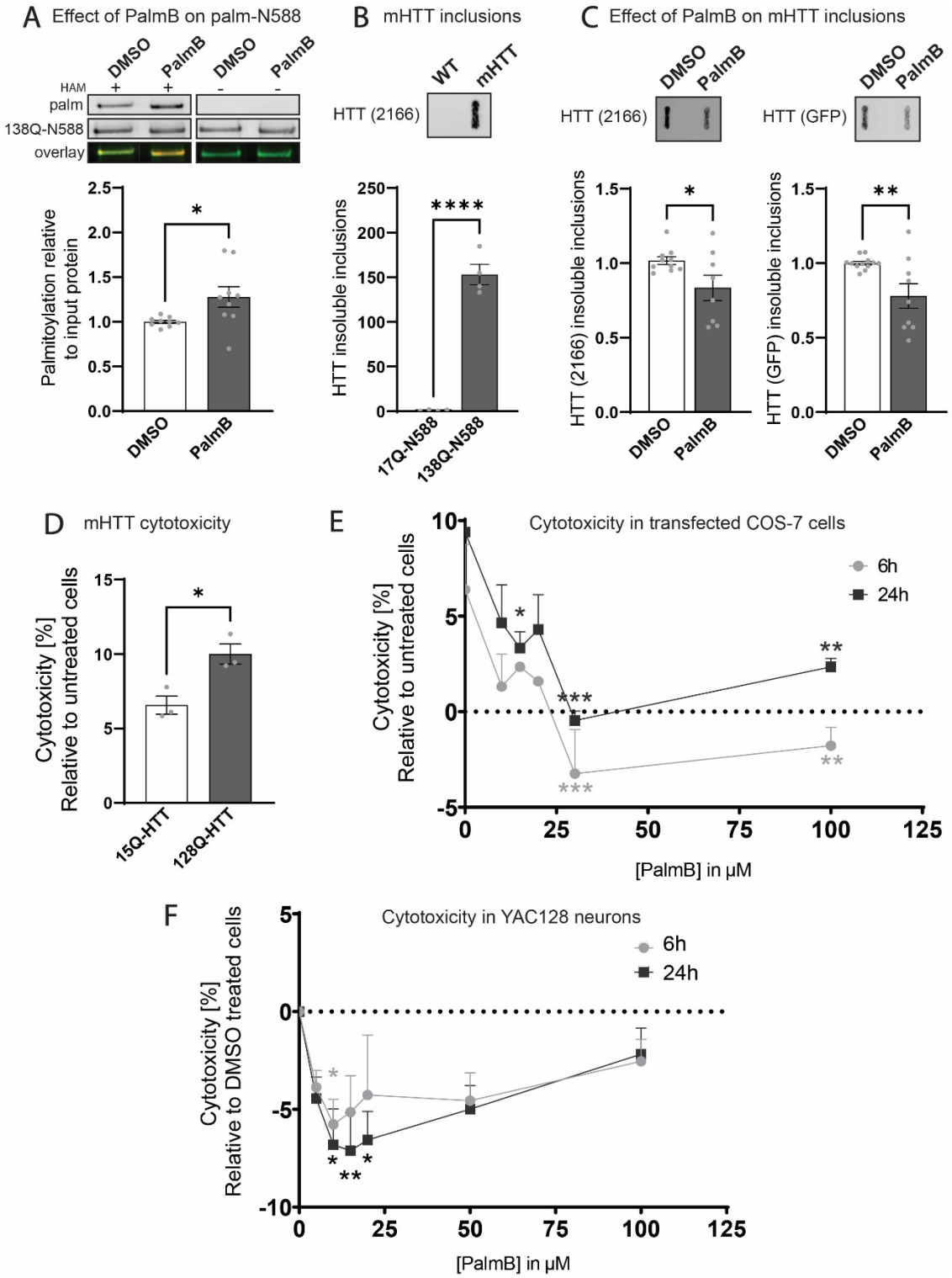

<u>Figure 6</u> - Inhibition of APTs with Palmostatin B reduces mHTT insoluble inclusions in COS-7 cells and mHTT-induced cytotoxicity in COS-7 cells and YAC128 cortico-striatal primary neurons.

1111 COS-7 cells were transfected at t=0h with 138Q-HTT$_{1-588}$-YFP (138Q-N588-YFP)
1112 construct, treated with 15 µM PalmB at t=24h and 48h post-transfection and harvested at
1113 t=72h.

1114 (**A**) Cell lysates were subjected to ABE assay to measure palmitoylated HTT. HTT was
1115 immunoprecipitated with anti-GFP antibodies and detected with MAB2166 for HTT and
1116 streptavidin for palmitoylated protein. HTT palmitoylation level was calculated as a ratio
1117 of palmitoylation signal over total HTT protein and expressed relative to palmitoylation in
1118 the DMSO control group.

1119 (**B-C**) Insoluble mHTT inclusions were monitored by filter retardation assay and
1120 immunodetection with anti-HTT (MAB2166) or GFP antibodies. The amount of
1121 aggregates retained on the filter is expressed relative to (**B**) 17Q-N588-YFP or (**C**) to the
1122 DMSO treated group.

1123 (**D**) Expression of full length 128Q-HTT in COS-7 cells increased cytotoxicity compared
1124 to 15Q-HTT expression. COS-7 cells seeded in 96-well pates were transfected with WT
1125 (15Q) or mutant (128Q) full length HTT for 24h. LDH activity in conditioned media was
1126 measured using the CyQUANT cell proliferation assay. Cytotoxicity (%) is expressed
1127 relative to untreated and non-transfected cells.

1128 (**E**) Cytotoxicity in COS-7 cells transfected for 24h with full length 128Q-HTT and treated
1129 with DMSO or PalmB (InSolution at 10, 15, 20, 30 and 100 µM) for 6 or 24h was assessed
1130 using the LDH activity assay (n=3). Cytotoxicity (%) is expressed relative to untreated and
1131 non-transfected cells. Negative cytotoxicity values correspond to a protective effect.

1132 (**F**) Cytotoxicity in YAC128 cortico-striatal primary neurons at DIV15 treated with DMSO
1133 or PalmB (InSolution at 5, 10, 15, 20, 50 and 100 µM) for 6 or 24h, using the LDH activity
1134 assay (n=4). Cytotoxicity (%) is expressed relatively to YAC128 neurons treated with
1135 DMSO. Negative cytotoxicity corresponds to a protective effect. Negative cytotoxicity
1136 values correspond to a protective effect.

1137 Statistical analysis: Student's T-test (**A**) p=0.029, (**B**) p<0.0001, (**C**) MAB2166, p=0.038
1138 and GFP, p=0.0065. (**D**) p=0.019. 2-way ANOVA: (**E**) Interaction, p=0.90, PalmB effect,
1139 p<0.0001, Treatment duration, p=0.0033; (**F**) Interaction, p=0.97; PalmB, p=0.0014;
1140 Treatment duration, p=0.29. Stars indicate Dunnett's test results compared to respective
1141 DMSO control.

1142 **Table 1 – List of reagents and chemicals used and application**

1143

	Reagent	Company	Catalogue #
Cell Culture Medium	DMEM without methionine and cystine	ThermoFisher Scientific	21013024
	DMEM/F12	ThermoFisher Scientific	11320033
	Dulbecco's Modified Eagle (DMEM)	ThermoFisher Scientific	11960044
	Neurobasal (NB)	ThermoFisher Scientific	21103049
	RPMI 1640	ThermoFisher Scientific	11875093
	mTeSR™1	STEMCELL Technologies	05850
Cell Culture Reagents	APT1 Inhibitor, palmostatin B	MilliporeSigma	178501
	B27 supplement	ThermoFisher Scientific	17504044
	Corning™ Matrigel™ hESC-Qualified Matrix	Fisher Scientific	354277
	Charcoal stripped FBS	ThermoFisher Scientific	12676029
	Dimethyl sulfoxide (DMSO)	MilliporeSigma	D2650
	DNase I, RNase-free	ThermoFisher Scientific	EN0525
	Fetal Bovine Serum	ThermoFisher Scientific	12483020
	GlutaMAX	ThermoFisher Scientific	35050061
	Hank's balanced salt solution (HBSS) (10X)	ThermoFisher Scientific	14060040
	InSolution™ APT1 Inhibitor, palmostatin B	MilliporeSigma	508738
	Nunc™ EasYFlask™ 25cm^2	ThermoFisher Scientific	156367
	Penicillin-Streptomycin (10,000 U/mL)	ThermoFisher Scientific	15140122
	Phosphate-buffered saline (PBS) (10X)	ThermoFisher Scientific	70011044
	Poly-D-lysine hydrobromide	MilliporeSigma	P7886
	ReLeSR™	STEMCELL Technologies	05872
	Sodium pyruvate	ThermoFisher Scientific	11360070
	Trypsin-EDTA (0.25%), phenol red	ThermoFisher Scientific	25200056
	Trypsin-EDTA (0.05%), phenol red	ThermoFisher Scientific	25300
	X-tremeGENE™ 9 DNA Reagent	MilliporeSigma	6365809001
	6-well, Nunclon delta surface plates	ThermoFisher Scientific	140685
	96-Well, Nunclon Delta-Treated plate	ThermoFisher Scientific	167425
Palmitoylation Assays	Biotin Azide	ThermoFisher Scientific	B10184
	Click Tag™ Palmitic Acid Alkyne	Cayman Chemical	13266
	EZ-Link BMCC-Biotin	ThermoFisher Scientific	21900
	Hydroxylamine hydrochloride	MilliporeSigma	255580
	N-ethylmaleimide (NEM)	MilliporeSigma	E3876
	Triton X-100	MilliporeSigma	T9284
	Tris(benzyltriazolylmethyl)amine (TBTA)	MilliporeSigma	678937
	Tris-carboxyethylphosphine (TCEP)	MilliporeSigma	C4706
	CYQUANT LDH cytotoxicity assay kit	ThermoFisher Scientific	C20303

	Benzonase® Nuclease	MilliporeSigma	E1014-25KU
	Cellulose acetate (OE66) membrane	MilliporeSigma	WHA10404180
Immunoblotting	Protran WB membranes, nitrocellulose	MilliporeSigma	GE10600000
	Dithiothreitol (DTT)	MilliporeSigma	3483-12-3
	Dynabeads™ Protein G	ThermoFisher Scientific	10003D
	Gel Cassettes, mini, 1.5 mm	ThermoFisher Scientific	NC2015
	NuPAGE LDS Sample Buffer (4X)	ThermoFisher Scientific	NP0007
	Invitrogen UltraPure TEMED	ThermoFisher Scientific	15524010
	NuPAGE Novex 3-8% Tris-Acetate gels	ThermoFisher Scientific	EA0375
	Protein Assay Reagent A	Bio-Rad	5000113
	Protein Assay Reagent B	Bio-Rad	5000114
	PureProteome magnetic beads	MilliporeSigma	LSKMAGAG02
	Roche complete Protease Inhibitor Cocktail	MilliporeSigma	11836145001
	Sodium dodecyl sulfate (SDS)	ThermoFisher Scientific	BP166-500
	2% Bis Solution	Bio-Rad	1610142
	30% Acrylamide/Bis Solution, 29:1	Bio-Rad	1610156
	40% Acrylamide Solution	Bio-Rad	1610140

1144

1145 **Table 2 – List of antibodies used and application**

Target (clone)	Species	Type	Supplier	Catalogue AB Registry Reference	Application	Dilution	Volume*
HTT (1HU-4C8)	Mouse	Monoclonal	Sigma-Aldrich	MAB2166 AB_2123255	WB	1:1,000	-
					IP	-	2 µL
HTT (D7F7)	Rabbit	Monoclonal	Cell Signaling Technology	5656 AB_10827977	WB	1:1,000	-
HTT (BKP1/HD46)	Rabbit	Polyclonal	in-house	(Kalchman et al., 1997)	IP	-	2 µL
					WB	1:400	-
HTT	Rabbit	Polyclonal	Sigma-Aldrich	H7540 AB_1840946	WB	1:1,000	-
					IP	-	2 µL
Streptavidin	-	Conjugated to AF-680	Invitrogen	S-32358	WB	1:5,000	-
PSD95 (7E3-1B8)	Mouse	Monoclonal	Invitrogen	MA1-046 AB_2092361	WB	1:1,000	-
PSD95	Rabbit	Polyclonal	in-house	-	IP	-	5 µL
GAD65	Rabbit	Polyclonal	Sigma-Aldrich	ABN101	WB	1:1,000	-
	Mouse	Monoclonal	DSHB	GAD-6 AB_2314499	IP	-	3 µL
SNAP25	Rabbit	Polyclonal	Synaptic Systems	111-002 AB_887790	WB	1:1,000	-
SNAP25 (SMI 81)	Mouse	Monoclonal	BioLegend	836303 AB_2715864	IP	-	3 µL
GFP	Rabbit	Polyclonal	Eusera	EU2	WB	1:5,000	-
					IP	-	0.75 µL
Mouse IgM (µ chain specific)	goat	-	Rockland Immuno-chemicals	92632210	WB (secondary)	1:5,000	-
Rabbit IgG	goat	-		926-32211	WB (secondary)	1:5,000	-

1146 *Volume of antibodies used for 20 µL of Dynabeads and 200 µg – 1 mg proteins

1147 **Table 3 – HD mouse lines used for palmitoylation assays**

Mouse model	Line	Reference	Promoter	Transgene product	CAG repeat length	Endogenous product
YAC128	53	(Slow et al., 2003)	Human HTT promoter and RE (24 kb upstream, 117 kb downstream)	full length human mHTT	128	2 copies of 7Q Htt
YAC18	60			2 copies of full length human wtHTT	18	2 copies of 7QnHtt
YAC128	55			2 copies of full length human mHTT	128	2 copies of 7Q Htt
BACHD	LA	(Gray et al., 2008)	Human HTT promoter and RE (20 kb upstream, 50 kb downstream)	full length human mHTT	97	2 copies of 7Q Htt
Hu18/18	KLAY	(Southwell et al., 2013)	Human HTT promoter and RE (20 kb upstream, 50 kb downstream)	full length human wtHTT	18	-
Hu97/18	KLAY			full length human WT and mHTT	97/18	-
Hu21/21	KT53	(Southwell et al., 2017)	Human HTT promoter and RE (24 kb upstream, 117 kb downstream)	full length human wtHTT	21	-
Hu128/21	KT53			full length human wt and mHTT	128/21	-

1148

1149

1150 **Table 4 – Lymphoblastoid cell lines from Coriell Biorepositories**

Catalog ID	Haplotype U/L	Status	Race	Age (years)	Sex	Family	CAG Lower	CAG Upper
GM07029		Control	Caucasian	47	Male	N/a	15	17
GM12716		Control		N/a	Male	1358	15	19
GM02160		Control		21	Male	109	16	17
GM02170		Control		22	Female	111	17	17
GM03863		Control		24	Female	268	17	17
GM03867	N/a	HD	Caucasian	26	Female	268	21	43
GM04023	C/A2	HD		28	Female	587	18	44
GM02176	A1/C	HD		26	Male	110	18	44
GM02150	A2/C	HD		26	Female	108	18	45
GM03620	A1/C	HD		29	Female	110	18	59
GM04724	A3/C	HD		19	Female	691	15	67
GM13509	A3/C	HD		N/a	Female	2706	15	66
GM04282	A3/A4	HD		20	Male	690	17	71

1151

1152

1153

1154 **<u>Table 5</u> – Isogenic HD patient-derived hiPSCs lines**

Cell type	Line	Reference	CAG repeat length
iPSCs	Parental control line (H9)	(Ooi et al., 2019)	30
	IsoHD lines		45
			65
			81
	Parental HD line (CAG180)	(Xu et al., 2017)	180
	Corrected line (HD-C#2)		18

1155